

Three-Nucleon Force Effects in Nucleon Induced Deuteron Breakup: Predictions of Current Models (I)

J. Kuroś-Żołnierczuk¹, H. Witała¹, J. Golak^{1,2}, H. Kamada³, A. Nogga⁴, R. Skibiński¹,
W. Glöckle²,

¹*M. Smoluchowski Institute of Physics, Jagiellonian University, Reymonta 4, 30-059 Kraków, Poland*

²*Institut für Theoretische Physik II, Ruhr Universität Bochum, D-44780 Bochum, Germany*

³*Department of Physics, Faculty of Engineering, Kyushu Institute of Technology
1-1 Sensucho, Tobata, Kitakyushu 804-8550, Japan*

⁴*Department of Physics, University of Arizona, Tucson, Arizona, 85721, USA
(November 4, 2018)*

Abstract

An extensive study of three-nucleon force effects in the entire phase space of the nucleon-deuteron breakup process, for energies from above the deuteron breakup threshold up to 200 MeV, has been performed. 3N Faddeev equations have been solved rigorously using the modern high precision nucleon-nucleon potentials AV18, CD Bonn, Nijm I, II and Nijm 93, and also adding 3N forces. We compare predictions for cross sections and various polarization observables when NN forces are used alone or when the 2π -exchange Tucson-Melbourne 3NF was combined with each of them. In addition AV18 was combined with the Urbana IX 3NF and CD Bonn with the TM' 3NF, which is a modified version of the TM 3NF, more consistent with chiral symmetry. Large but generally model dependent 3NF effects have been found in certain breakup configurations, especially at the higher energies, both for cross sections and spin observables. These results demonstrate the usefulness of the kinematically complete breakup reaction in testing the proper structure of 3N forces.

21.30.-x, 21.45.+v, 25.10.+s, 24.70.+s

I. INTRODUCTION

The nucleon induced deuteron breakup reaction together with elastic nucleon-deuteron (Nd) scattering have been considered for long as a valuable tool to test the three-nucleon (3N) Hamiltonian, in particular to shed light on the importance and structure of a three nucleon force (3NF) in the potential energy of the 3N system [1,2]. However, up to recently difficulties in solving rigorously 3N equations in the continuum for realistic forces prohibited clear statements in such a study. The rapid progress in supercomputer technology made it now possible to gain numerically exact solutions of 3N Faddeev equations for any nucleon-nucleon (NN) interaction, even including a 3NF [3].

Present day models of NN interactions, mostly phenomenological and/or based on a meson exchange picture, have achieved a high degree of maturity. It was possible by adjusting their parameters to describe with high precision ($\chi^2/data \approx 1$) NN data in the large energy range from threshold to about 350 MeV [4–7]. These so called realistic potentials AV18 [5], CD Bonn [6,7], Nijm I, II, and Nijm 93 [4], are now extensively used in few-nucleon studies. Recent developments of chiral perturbation theory lead to NN potentials, where the one- and multi-pion exchanges are treated unambiguously according to chiral symmetry [8–16]. Therefore the theoretical uncertainties of meson exchange based models have been at least partially removed and this step puts the theory of nuclear forces on a more solid basis. First successful applications of these interactions in 3N and 4N systems have already demonstrated their power in interpreting and describing the data [17–21]. In this paper, however, we shall only apply the above mentioned high-precision NN interactions.

This present state of NN potential models, describing NN data perfectly, suggests now, when going to systems with more than two nucleons, to concentrate on the significance and properties of many-body force contributions to the nuclear Hamiltonian. In case of three nucleons the first indication on the importance of 3NF contributions came from ^3He and ^3H bound state studies. All realistic NN potentials are unable to reproduce their experimental binding energies leading to a ^3He and ^3H underbinding of the order of $0.5 \div 1$ MeV [22]. This clear cut underbinding exists also for ^4He where it amounts to $2 \div 4$ MeV [22–24]. Also for higher mass nuclei up to $A=8$, where stochastic techniques must be applied, realistic NN forces failed to provide the experimental binding energies [25,26].

A natural step to explain this underbinding was to consider 3NFs in the nuclear Hamiltonian. Presently, the most often used dynamical process is the 2π -exchange between three nucleons. An important dynamical ingredient in that process is, as suggested long time ago by the Fujita-Miyazawa 3NF [27], an intermediate excited nucleon state Δ . It was augmented later by further ingredients leading to the Urbana IX [28] and Tucson-Melbourne (TM) [29] 3NFs, which are mostly used in present day few-nucleon calculations. It was possible by properly adjusting the parameters of these 3NFs to get essentially correct 3N and 4N binding energies. Also a fairly successful description of low energy bound state energies of up to $A=8$ nuclei resulted when adding 3NFs. This was recently improved by adding further 3NFs related to three-pion exchange with intermediate Δ 's [30]. In the present exploratory investigation we shall not yet include this newest generation of 3NFs.

Though this first signal on 3NF effects, resulting from discrete states, is important an even more sensitive and detailed investigation of 3NF properties can be carried through in scattering processes, where already a rich set of spin observables has been measured

and further data are expected to come [31–34]. From the theoretical side one can make exact predictions for these observables using nuclear forces in all their complexities [3]. Experimentally one can access nowadays spin observables in elastic Nd scattering where in the initial states the deuteron and/or the nucleon is polarized and where in the final state the polarizations of the outgoing particles can also be measured [35–43]. This together with cross sections leads to a very rich spectrum of observables in Nd elastic scattering and the Nd breakup process. Such a set of observables will be a solid basis to test the 3N Hamiltonian. Using available model Hamiltonians one can provide guidance to select specific observables and energies which are most appropriate to see 3NF properties. In [44] such a study has been performed for elastic Nd scattering. It was shown that the current 3NF models exhibit a lot of effects and more data are needed to provide constraints on the theoretical models of 3NFs. First data sets [31,35,38–40] in elastic Nd scattering showed both, successes and failures of present day 3NF models combined with the realistic NN forces. It is the aim of this paper to probe the cross section and several spin observables of the kinematically complete Nd breakup process against sensitivity to 3NFs combined with the high-precision NN interactions. In a following paper (II) already existing data will be compared to those model predictions.

For the convenience of the reader we briefly review in Section II our theoretical formalism for the 3N continuum and display the 3NF models which are presently in vogue and which we use. Our predictions for quite a few breakup observables based on various nuclear force combinations are presented in Section III. While in this Section we investigate the full 3N breakup phase space we concentrate on a subset of breakup configurations in Section IV according to the experimental restrictions imposed in an ongoing experiment at KVI [33,45]. We conclude in Section V.

II. THEORETICAL FORMALISM AND 3NF MODELS

We refer to [3] for a general overview on 3N scattering and specifically for our way to formulate it. The inclusion of 3NFs follows [46]. This is a direct generalization of what is being used for the 3N bound state [47]. We define an amplitude T via our central Faddeev-like equation:

$$T = tP\phi + (1+tG_0)V_4^{(1)}(1+P)\phi + tPG_0T + (1+tG_0)V_4^{(1)}(1+P)G_0T \quad (1)$$

The initial channel state ϕ is composed of a deuteron and a momentum eigenstate of the projectile nucleon. The two-body t -operator is denoted by t , the free 3N propagator by G_0 and P is the sum of a cyclical and an anticyclical permutation of three particles. The 3N force V_4 can always be decomposed into a sum of three parts:

$$V_4 = V_4^{(1)} + V_4^{(2)} + V_4^{(3)}, \quad (2)$$

where $V_4^{(i)}$ is symmetrical under the exchange of the nucleons jk with $j \neq i \neq k$. As seen in Eq. (1) only one of the three parts occurs explicitly, the others via the permutations contained in P .

The physical breakup amplitude is given via

$$U_0 = (1 + P)T. \quad (3)$$

The Faddeev-like integral equation (1) has the nice property that the terms resulting by iteration and inserted into Eq. (3) yield the multiple scattering series, which gives transparent insight into the reaction mechanism.

The definition of the various spin observables can be found in [3,48,49]. We shall encounter nucleon and deuteron vector analysing powers A_y and $A_y^{(d)}$, where in the initial state either the nucleon or the deuteron is polarized. Further, the deuteron can be tensor polarized in the initial state leading to the three tensor analysing powers T_{2k} ($k = 0, 1, 2$) or the corresponding cartesian analyzing powers A_{ij} ($i, j = x, y, z$).

We concentrate in this study on the kinematically complete 3N breakup. The final 3N state of this reaction is specified by nine momentum components. In such an experiment the energies and directions (polar and azimuthal angles θ_i and ϕ_i) of two outgoing nucleons ($i = 1, 2$) are measured. This together with restrictions imposed by energy and momentum conservation lead to a correlation of the measured energies E_1 and E_2 , causing them to lie on a kinematical curve (S-curve) in the $E_1 - E_2$ plane. All observables will be presented as a function of the arc length S related to a point along this kinematical curve. It is a matter of convention to choose the location of $S=0$ on the S-curve and we use the one defined in Ref. [3].

As NN forces we use the five realistic NN interactions mentioned in the introduction. They are combined with 3NF models. The 2π -exchange TM model [29] has been around for quite some time and is based on a low momentum expansion of the $\pi - N$ off- (the mass-) shell scattering amplitude. It has the following form:

$$V_4^{(1)} = \frac{1}{(2\pi)^6} \frac{g_{\pi NN}^2}{4m_N^2} \frac{\vec{\sigma}_2 \cdot \vec{Q}}{\vec{Q}^2 + m_\pi^2} \frac{\vec{\sigma}_3 \cdot \vec{Q}'}{\vec{Q}'^2 + m_\pi^2} H(\vec{Q}^2) H(\vec{Q}'^2) \times \\ \times \left\{ \vec{\tau}_2 \cdot \vec{\tau}_3 \left(a + b\vec{Q} \cdot \vec{Q}' + c(\vec{Q}^2 + \vec{Q}'^2) \right) + d i\vec{\tau}_3 \times \vec{\tau}_2 \cdot \vec{\tau}_1 \vec{\sigma}_1 \cdot \vec{Q} \times \vec{Q}' \right\}. \quad (4)$$

The elements of the underlying Feynman diagram are obvious: the two-pion propagators depending on the pion momenta \vec{Q} and \vec{Q}' , the strong form factors combined into the two H -functions and most importantly the parameterization of the πN amplitude inside the curly bracket which is combined with the isospins $\vec{\tau}_2$ and $\vec{\tau}_3$ of the two accompanying nucleons. The H -functions are parameterized as:

$$H(\vec{Q}^2) = \left(\frac{\Lambda^2 - m_\pi^2}{\Lambda^2 + \vec{Q}^2} \right)^2 \quad (5)$$

In what we denote by the TM 3NF we use the original parameters $a = 1.13/m_\pi$, $b = -2.58/m_\pi^3$, $c = 1.0/m_\pi^3$, $d = -0.753/m_\pi^3$ where $m_\pi = 130.6$ MeV [50]. The still very demanding computer resources prevented us to use the recently updated values [51] which, however, differ only slightly from the one we use and we do not expect significant changes. The b - and d -terms are mostly determined by an intermediate Δ in a static approximation. The a - and c -terms are related to S -wave πN scattering. The cut-off parameter Λ is used to adjust the ^3H binding energy separately for different NN forces [22]. In units of the pion

mass m_π we find the Λ to be: 4.856, 5.215, 5.120, 5.072, and 5.212 when the TM 3NF is combined with CD Bonn, AV18, Nijm I, II, and Nijm 93, respectively.

Of course in a meson exchange picture additional processes should be added containing different mesons like $\pi - \rho$, $\rho - \rho$, etc.; different intermediate excited states might also play a role [52]. To some extent 3NF models with respect to those extensions have already been developed and applied [53–57]. Our adjustment of Λ is a very rough manner to take other processes into account. Further studies incorporating these additional 3NFs should be performed both for elastic Nd scattering and the breakup process.

The parameterization of the TM 3NF has been criticized, since it violates chiral symmetry [58,59]. A form consistent with chiral symmetry (though still incomplete to that order in the appropriate power counting) is obtained by keeping the long range part of the c -term leading to a changed parameter $a' \equiv a - 2m_\pi^2 = -0.87/m_\pi$ [58,59] and dropping the short range part. This essentially means a change of sign for a . This form will be called TM' later on. The corresponding Λ -value, when TM' is used with the CD Bonn potential, is $\Lambda = 4.593$.

The two-meson exchange 3NF has been also studied by Robilotta *et al.* [60] leading to the Brazilian 3NF. It is similar to the one of TM and also the results gained for 3N observables [61] are similar to the ones for the TM 3NF. In this paper we do not take that force into account. Instead we included the Urbana IX 3NF [28], which is intensively used in the Urbana-Argonne collaboration. That force is based on the old Fujita-Miyazawa ansatz [27] of an intermediate Δ occurring in the two-pion exchange and is augmented by a spin and isospin independent short range piece. It has the form

$$V_4^{(1)} = A_{2\pi} \left[\{X_{12}, X_{13}\} \{\vec{\tau}_1 \cdot \vec{\tau}_2, \vec{\tau}_1 \cdot \vec{\tau}_3\} + \frac{1}{4} [X_{12}, X_{13}] [\vec{\tau}_1 \cdot \vec{\tau}_2, \vec{\tau}_1 \cdot \vec{\tau}_3] \right] + U_0 T_\pi^2(r_{12}) T_\pi^2(r_{13}), \quad (6)$$

where $\{, \}$ and $[,]$ are anticommutator and commutator brackets and X_{ij} is defined as:

$$X_{ij} = Y_\pi(r_{ij}) \vec{\sigma}_i \cdot \vec{\sigma}_j + T_\pi(r_{ij}) S_{ij} \quad (7)$$

Here σ_i is a nucleon spin operator, S_{ij} is the standard tensor force, the $T(r_{ij})$ and $Y(r_{ij})$ are functions of the distance r_{ij} between nucleons i and j , that are associated with the Yukawa and tensor part of the one-pion-exchange interaction

$$Y_\pi(r) = \frac{e^{-m_\pi r}}{m_\pi r} (1 - e^{-cr^2}), \quad (8)$$

$$T_\pi(r) = \left[1 + \frac{3}{m_\pi r} + \frac{3}{(m_\pi r)^2} \right] \frac{e^{-m_\pi r}}{m_\pi r} (1 - e^{-cr^2})^2, \quad (9)$$

quenched via a short-range cut-off function $(1 - e^{-cr^2})$ with $c=2.1 \text{ fm}^{-2}$ [62]. The parameters $A_{2\pi}$ and U_0 were chosen to reproduce the experimental ${}^3\text{H}$ binding energy and to obtain the empirical equilibrium density of nuclear matter when this 3NF model is used with the AV18 potential. Their values for model IX are $A_{2\pi} = -0.0293 \text{ MeV}$ and $U_0 = 0.0048 \text{ MeV}$ [28].

Since we work in momentum space using a partial wave expansion, the form given in Eq. (6) has to be rewritten. This has been done in [44].

Since there is no apparent consistency of the mostly phenomenological realistic NN forces and the 3NF models, we test various combinations thereof. In all cases, however, we require that the particular force combination should reproduce the experimental triton binding energy. Some of the 3N observables scale with the triton binding energy [63]. The adjustment to the triton binding energy has the advantage that our investigation is not misled by these scaling effects.

With respect to the intermediate Δ one should say that very likely the static approximation is not justified and the Δ should be allowed to propagate like the nucleon. This has been pursued intensively, for instance, by the Hannover group [64] and their recent work has been also devoted to the 3N continuum [65].

In view of all that, it is quite clear that our present study is not at all complete but can at least provide some insight into effects specific 3NF models generate for breakup observables.

III. PREDICTIONS OF 3NF EFFECTS

Since we would like to cover a wide range of incoming nucleon energies, ranging from just above the Nd breakup threshold up to 200 MeV, it is necessary to take a sufficient number of partial waves into account to guarantee converged solutions of the Faddeev equations. In all presented calculations we went up to the two-nucleon subsystem total angular momentum $j_{max} = 5$. This corresponds to a maximal number of 142 partial wave states (channels) in the 3N system. We checked that the convergence has been achieved by looking at the results obtained for $j_{max} = 6$, which increases the number of channels to 194. This convergence check refers to a calculation without a 3NF. The inclusion of 3NFs has been carried through for all total angular momenta of the 3N system up to $J = 13/2$. These high angular momenta are required at the higher energies ≥ 100 MeV. The longer ranged 2N interactions require states up to $J = 25/2$ at the higher energies in order to get converged results.

A phenomenological criterion for 3NF effects is that they lie outside of the spread of the five realistic NN force predictions only. This spread will be indicated by a band (called the “2N” band). Unfortunately we cannot include the pp Coulomb force effects. At the higher energies, however, those effects should be small. Also in case of AV18 we do not take the various electromagnetic corrections into account, which leads among possibly other effects to a slightly wrong deuteron binding energy ($E_b = 2.242$ instead of 2.225 MeV). This shifted E_b -value, however, has only a small effect on our results, which is mostly of kinematical origin. Also the NN-phase shifts, obtained without those additional terms, differ only slightly from the standard ones. The kinematical effect also leads to a slight shift in the position of the S-curve.

To investigate 3NF effects we combine the TM 3NF with the five NN forces forming a second band (called the “2N+TM” band). In all cases the cut-off value Λ in Eq. (5) has been adjusted separately for each NN force to the ^3H binding energy [66] as given in the previous Section. Since that interplay is a purely phenomenological step, the outcome is theoretically not under control and we combine all the results into a second band. In addition, we want to compare the TM 3NF and the modified TM’, which is more consistent with chiral symmetry. We combine TM’ with CD Bonn and display the results as a dashed

curve. Finally we compare the AV18 with the Urbana IX 3NF what is presented as a solid line. There are clearly more combinations possible but we felt this to be sufficient to get an orientation on the magnitudes of the effects.

Before starting to investigate exclusive breakup configurations with large 3NF effects, it is interesting to look at the elastic scattering and breakup contributions to the total cross section for neutron-deuteron (nd) scattering. Fig. 1 shows the total cross section σ_{tot} , predicted by the CD Bonn potential, as a function of the incoming neutron laboratory energy up to 300 MeV together with the contributions coming from elastic scattering and the breakup processes. It is seen that the total elastic cross section decreases rapidly with increasing energy of the incoming neutron. At about 50 MeV the breakup contributes already $\sim 50\%$ to the total cross section. At higher energies it dominates the total cross section and at about 200 MeV the elastic scattering contributes only $\sim 20\%$ to the total cross section. This picture does not depend on the choice of the NN potential used: the theoretical results for the nd total elastic and breakup cross sections are stable under the exchange of the realistic NN potentials. The differences are of the order of 1%.

In Figs. 2-4 we compare the theoretical predictions with the experimental data. There is a good agreement between the “pure” NN theory and the data up to ~ 50 MeV for all three total cross sections. At higher energies the data exist only for σ_{tot} and the theory begins to underestimate the data (about 2% at around 100 MeV and about 13% at ~ 300 MeV) [67,68].

In order to see the influence of 3NFs, we calculated the total cross section for nd scattering combining some of the NN potentials and 3NF models as described above. We see, adding a 3NF increases the value of the different total cross sections and shifts the theoretical predictions closer to the data (it is clearly visible for $E_{lab} \gtrsim 100$ MeV in Fig. 5). The predictions obtained with different 3NF models are practically the same.

In order to quantify the effect of a 3NF on the total cross sections we calculated its relative contributions in the corresponding processes as:

$$\Delta\sigma_i^{3NF} = \left| \frac{\sigma_i^{(2N)} - \sigma_i^{(2N+TM)}}{\sigma_{tot}^{(2N)}} \right| \times 100\% \quad (10)$$

where $\sigma_i \equiv \sigma_{tot}, \sigma_{tot}^{elas}, \sigma_{tot}^{br}$. As can be seen from Fig. 6, the 3NFs enhance the nd total cross section only by about up to 5%. This enhancement is practically independent from the particular 3NF used and for energies above 100 MeV changes only slightly with energy. Due to the drastically diminishing contribution of the total elastic cross section most of the 3NF effects at higher energies must occur in the breakup process. Since the total breakup cross section is dominated by the quasi free scattering, for which 3NF effects are negligible [3,69], it follows, that at higher energies 3NF effects must be found in other breakup configurations, possibly just in some specific geometries. It is one of the aims of this paper to investigate this conclusion in detail.

As can be seen from Fig. 5, addition of a 3NF only partially removes the discrepancy between data and theory. At higher energies one has to expect that relativistic effects might appear. A generally accepted framework for carrying out relativistic 3N calculations does not yet exist. An estimation of these effects due to proper relativistic treatment of the kinematics while keeping the (non-relativistic) scattering amplitudes unchanged was done in [68]. It was found, that such relativistic effects enhance the nd total cross section by

about 7% at 250 MeV while being much smaller at lower energies. These corrections bring the theoretical predictions for the nd total cross section much closer to the data.

In the following we restrict the study of 3NF effects to the nd breakup reaction. Contrary to elastic scattering, where the description of the two-body final state requires only one variable (e.g. the c.m. angle θ), the 3N final state of the breakup process is kinematically much more complex and requires five parameters to be described completely. The possibility to choose very many specific kinematical geometries and energy distributions for the three outgoing nucleons allows to probe the 3N Hamiltonian in greater detail.

Our goal is to scan the full breakup phase space for the configurations which exhibit large 3NF effects in some observables. In order to cover the broad range of incoming energies, we took, as representatives, the following laboratory energies: 13, 65, 135, and 200 MeV.

As a first exploratory study, we calculated the five-fold differential cross section $\sigma \equiv \frac{d^5\sigma}{dS d\Omega_1 d\Omega_2}$, and the analyzing powers $A_y, A_x, A_z, A_y^{(d)}, A_{yy}, A_{xz}, A_{xx}$ using the CD Bonn NN potential with and without the TM 3NF. The observables were tabulated as a function of $E_1, E_2, \theta_1, \theta_2$ and $\phi_{12} \equiv \phi_1 - \phi_2$, varying θ_i in steps of 5° , ϕ_{12} in steps of 10° and taking a step along the S-curve, $\Delta S(E_1, E_2) = 1$ MeV, over the full phase space.

In order to check if the chosen grid over the full phase space was sufficiently dense we calculated:

$$\sigma_{tot}^{scan} \equiv \sum_{i=1}^N \left(\int d\Omega_1 d\Omega_2 dS \frac{d^5\sigma}{d\Omega_1 d\Omega_2 dS} \right)_i \quad (11)$$

where N is the number of the calculated configurations. In Tab. I the values of σ_{tot}^{scan} are compared with the total breakup cross section σ_{tot}^{br} . The difference between σ_{tot}^{br} and σ_{tot}^{scan} is smaller than 5%, what gives a strong support that our grid is sufficiently dense.

In order to discover interesting cases we looked for configurations with the largest differences between observables predicted with the CD Bonn alone and when the TM 3NF has been included. The influence of the TM 3NF can be quantitatively defined by the relative difference δO of the observable $O = \sigma, A_y, A_x, A_z, A_y^{(d)}, A_{yy}, A_{xz}, A_{xx}$ at a given phase space point $(E_1, E_2, \theta_1, \theta_2, \phi_{12})$ when the TM 3NF is switched on

$$\delta O(E_1, E_2, \theta_1, \theta_2, \phi_{12}) \equiv \left| \frac{O^{(2N)} - O^{(2N+TM)}}{O^{(2N)}} \right| \times 100\% \quad (12)$$

Here $O^{(2N)}$ and $O^{(2N+TM)}$ are the predictions for the particular observable O using the CD Bonn potential alone and including in addition the TM 3NF. In the case of analyzing powers, due to experimental limitations only kinematical points have been considered for which $|A_i^{(2N)}| \geq 0.05$.

In order to get insight into the limitations imposed by the experimental conditions in detecting interesting cases we performed the search in three steps. First, for each observable O at each energy we searched over the entire grid of the phase space for those points where δO achieves its maximum value ΔO :

$$\Delta O \equiv \max[\delta O(E_1, E_2, \theta_1, \theta_2, \phi_{12})]$$

The resulting ΔO 's are presented in the rows labeled *all* in Tab. II. Second, bearing in mind that we look for effects that should be experimentally accessible, we searched for the

maximum of δO only at phase space points for which the cross section $\sigma^{(2N)} \geq 0.01 \frac{mb}{sr^2 MeV}$ and this for at least 5 MeV along the S-curve (σ -cut). The resulting ΔO 's are shown in the rows labeled σ -cut. And finally, in addition to the σ -cut, we demand that the energies of the detected nucleons (E_1, E_2) must be greater than 15 MeV¹. The final ΔO 's are displayed in the third rows labeled $\sigma + E$ -cut. Supplementary, in the last column of Tab. II labeled N we present the number of configurations fulfilling without maximum requirements the three search restrictions: no restrictions, applying the σ -cut, and applying both, the σ - and E -cuts.

The cross section (σ -cut) and energy (E -cut) threshold values are based on current experimental conditions and limitations. We are aware that each of these values is somewhat arbitrary. We do not need to lower them, however, since as we show below the 3NF effects are already clearly visible under these restricted conditions.

As we can see in Tab. II the 3NF effects, in general, increase with the energy of the incoming nucleon. This tendency also holds after applying the σ -cut and the σ -cut together with the E -cut. The only exceptions are A_x (where the maximum value of ΔA_x including the cuts is at $E_{lab} = 65$ MeV) and A_y and A_{xx} (where the 3NF effects are largest at 135 MeV rather than at 200 MeV). The values of ΔO after applying both the σ - and E -cuts do not change in a considerable way but the number of configurations N decreases dramatically.

The polarization observables are particularly sensitive to the 3NF. Among them the tensor analyzing powers are especially interesting, showing large 3NF effects. The nucleon and deuteron vector analyzing powers ($A_y, A_y^{(d)}$) are good tools to test the 3NF as well. Predictions for the differential cross section are also very promising, especially at the energies 135 and 200 MeV. The 3NF influence is the least evident in A_z and A_x .

The next step in our analysis was to divide the phase space into regions according to certain values of $\delta O = \delta O(\theta_1, \theta_2, \phi_{12}, E_1, E_2)$ for our chosen observables. Of course, the regions where δO takes its largest values are of the strongest interest. In order to display these regions, we project them onto three planes: θ_1 - θ_2 , θ_1 - ϕ_{12} and E_1 - E_2 . Fig. 7 shows one example for $\Delta\sigma$ at 135 MeV. The three rows represent the three cut conditions described above and labeled as in Tab. II. Using the information from the first and the second column for $\Delta\sigma$, varying between 0 and 90%, one can locate the angular regions in phase space where $\Delta\sigma$ values of a certain magnitude can be found. The last column provides the additional information in the energy distribution. For example our sample plot shows one very promising configuration ($(\theta_1 \simeq 15^\circ, \theta_2 \simeq 15^\circ, \phi_{12} \simeq 0^\circ)$) with $\Delta\sigma \gtrsim 90\%$. Moreover that configuration survives all the applied cuts. The corresponding situation for A_{yy} is shown in Fig. 8. It is seen that 3NF effects are larger in magnitude and they occur in different regions of the phase space compared to the interesting ones for $\Delta\sigma$.

In this way we found at each energy the most promising configurations for each studied observable. It turned out that the influence of the 3NF is not limited to separate points but rather shows up in extended regions of phase space. Also the regions differ with the observable chosen.

Next we performed more detailed studies. For each observable and each energy we have chosen about 20 angular configurations and calculated the observable using the five high-

¹3 MeV for $E_{lab} = 13$ MeV

precision potentials. In the following figures they form the light shaded band. Then the TM 3NF was combined with all five NN potentials forming a second band (dark shaded band in the following). In addition, we regard the force combinations CD Bonn with TM' and AV18 with Urbana IX.

As a result of our study, we have a huge amount of information on the 3NF effects for each observable at each of the four energies. In the following, we present only general conclusions about each observable and we only show the most interesting configurations. More results and examples can be found in [69].

A. 3NF effects at 13 MeV

The case of 13 MeV serves as an example for 3NF effects in a low energy breakup process. From Tab. II it follows that for vector analyzing powers no significant 3NF effects are present. The values of ΔO for tensor analyzing powers and the cross section give some hope to find configurations with measurable 3NF effects. In Fig. 9 we show some examples in which we found the largest effects for the differential cross section, A_{xx} , A_{yy} and A_{xz} . Unfortunately, the spread in the predictions of various NN potentials can be as large as 10% and this is comparable in magnitude with the 3NF effects found. Therefore the conclusion is that the 3NF effects at 13 MeV are too small to be distinguished from the dependences on the NN force model.

B. 3NF effects at higher energies

To look for the magnitude of 3NF effects at higher energies we investigated each of the another eight observables listed above at 65, 135 and 200 MeV. We focus only on configurations which survive both the σ - and E -cuts, because our aim is to find regions of the phase space with large and measurable 3NF effects. In all cases, however, we checked if the rejected configurations contain interesting 3NF effects.

1. Differential cross section

At higher energies there are significant effects of 3NFs in the differential cross section. They are particularly large (more than 90%) in some configurations at 135 and 200 MeV.

Generally, in all phase space points studied adding the TM 3NF increases the value of the cross section at 135 and 200 MeV, whereas at 65 MeV we found configurations where the TM 3NF decreases σ . We show prominent cases in Fig. 10. We see that at 135 and 200 MeV $\delta\sigma \geq 60\%$ (in fact this happens not only for $\phi_{12} = 0^\circ$ but in a range as large as 20°). In the maxima of the cross sections the energies of two outgoing nucleons (E_1 and E_2) are comparable and together amount to about 80% of the total accessible energy. The “2N” and “2N+TM” bands are well separated.

Astonishingly, at 135 and 200 MeV the AV18+Urbana IX and CD Bonn TM' predictions, while close together, are distinctly different from all NN force combinations with TM.

2. Vector analyzing powers A_y and $A_y^{(d)}$

The 3NF effects for the nucleon and deuteron vector analyzing powers A_y and $A_y^{(d)}$ increase with energy and become quite large at higher energies in some specific configurations.

Most of these configurations are close to the so-called final state interaction (FSI) geometry, where the two outgoing nucleons have equal momenta. For example, at 200 MeV the value of $\delta A_y^{(d)}$ reaches about 350% for the $(\theta_1, \theta_2, \phi_{12}) = (25^\circ, 25^\circ, 0^\circ)$ configuration while in others $\delta A_y^{(d)} \leq 150\%$. Similarly, δA_y reaches the maximal value of nearly 200%, but only in few configurations goes above 140% (six for 135 MeV and three for 200 MeV). Figs. 11 and 12 show examples of the most interesting configurations at each energy. Despite the substantial broadening of both “2N” and “2N+TM” bands (especially at 65 MeV), the TM 3NF effects are clearly visible. At higher energies the predictions with and without TM 3NF have even different signs, both for A_y and $A_y^{(d)}$. We found also some configurations where the inclusion of the TM 3NF decreases the pure NN value of the analyzing powers from the positive value 0.2 to zero (e.g. $(15^\circ, 15^\circ, 20^\circ)$). Data from such configurations can be an excellent tool to test 3NF models.

We cannot draw any general conclusions about the predictions obtained using Urbana IX with AV18 and TM’ with CD Bonn, since they are quite different in various configurations. In addition they can be also quite different from the TM predictions.

3. Nucleon analyzing powers A_x and A_z

To get nonzero values for the nucleon analyzing powers A_x and A_z one has to go out of the reaction plane [48,49]. For both of them the 3NF effects are the smallest among all considered analyzing powers. Moreover, the largest δA_x value was found at 65 MeV and it decreases with increasing energy (assuming cuts). For A_z the maximum values of δA_z at 135 and 200 MeV are comparable ($\delta A_z \cong 60\%$) and they are larger than the corresponding value at 65 MeV ($\delta A_z \cong 20\%$). For A_z the assumed threshold value of $|A_z|$ ($|A_z| \geq 0.05$) is crucial because $|A_z|$ reaches measurable values only at higher energies. There this cut is not so decisive anymore because the maximum of $|A_z|$ is larger and approaches 0.45.

Again, we picked up the most promising configurations and show them in Figs. 13 and 14 for A_z and A_x , respectively. At all energies the “2N” and “2N+TM” bands are rather narrow and the 3NF effects are clearly visible. For A_x and A_z the Urbana IX and TM’ forces provide smaller 3NF effects.

4. Tensor analyzing powers

These spin observables appear to be the most sensitive to the 3NFs we used. For each of them the magnitude of 3NF effects increases strongly with the energy. There are extended regions of the phase space with large 3NF effects at each energy, what makes the investigation of A_{xx} , A_{yy} and A_{xz} extremely promising. At the highest energy there are a few configurations with especially large values of δA_i ($A_i = A_{yy}, A_{xx}, A_{xz}$). One distinguished example is A_{yy} for which δA_{yy} reaches the extremely large value of about 400% in the $(45^\circ, 45^\circ, 0^\circ)$ configuration (see Fig. 15). For this observable there are in addition

three configurations with $\delta A_{yy} \geq 250\%$. They are close to FSI geometries with comparable energies of the two outgoing nucleons. We found a similar behavior for A_{xx} and A_{xz} .

At the higher energies we even found several configurations with different signs for the “2N” and “2N+TM” bands what leads to a very big value of δA_i . However, they do not always represent the best region to investigate 3NF effects. For example, δA_{xx} at 200 MeV reaches the largest value for the $(145^\circ, 10^\circ, 180^\circ)$ configuration but the short length of the S-curve, where 3NF effects are large, makes this configuration hard to use for an experimental study. We have also found several configurations with large 3NF effects but the large spreads of “2N” and “2N+TM” bands inhibit the unambiguous conclusion about the significance of 3NF effects, e.g. for A_{xz} at 200 MeV in $(45^\circ, 45^\circ, 0^\circ)$ or configurations with largest δA_{yy} . On the other hand some of these configurations present themselves as excellent playground to look for differences between different models of NN interactions.

Figs. 15, 16 and 17 show our choice for the most sensitive configurations. The predictions using Urbana IX combined with AV18 and TM’ with CD Bonn are often close to each other and give smaller effects than with the TM 3NF.

IV. SEARCH FOR CONFIGURATIONS WITH LARGE 3NF EFFECTS IN THE $P(\vec{D}, PP)N$ BREAKUP AT 130 MEV

Awaiting results from a new experiment currently under way at KVI in Groningen [33], we calculated the differential cross section $\frac{d^5\sigma}{d\Omega_1 d\Omega_2 dS}$ together with vector and tensor analyzing powers $A_y^{(d)}$, A_{xx} , A_{yy} , A_{xz} for the $p(\vec{d}, pp)n$ breakup reaction at $E_d = 130$ MeV in the laboratory frame. All these observables are planned to be measured. The calculations were performed for 970 configurations covering the entire experimentally available phase space (the maximal available angle of the outgoing protons is $\theta = 76.9^\circ$ in the laboratory frame). We used the CD Bonn potential with and without the TM 3NF varying the angles θ_1 , θ_2 and ϕ_{12} in steps of 5° and the position on the kinematical locus $S(E_1, E_2)$ in steps of 1 MeV. This exploratory study with the only force combination CD Bonn and TM was performed in the same way as in the previous Section III and the results are presented in Tab. III. Again the tensor analyzing powers are the most sensitive observables to 3NFs. Then we performed in addition a more detailed study using all force combinations as in the previous Section.

A. Differential cross section

In the case of the differential cross section the experimentally required condition $E_i \geq 15$ MeV rejects a lot of very promising configurations with $\phi_{12} \leq 70^\circ$. Despite that, we found many configurations with 3NF effects in the region of the maximal values (see Tab. III). Very interesting configurations are $(\theta_1 \simeq 20^\circ, \theta_2 \simeq 20^\circ, \phi_{12} \geq 130^\circ)$ which correspond to the situation where one of the outgoing nucleons takes all accessible energy.

In Fig. 18 we show cross sections for three configurations revealing one of the largest 3NF effects. Only part of the allowed S-curve is presented, for which the energies of the protons fulfill the conditions $E_{1,2} \geq 15$ MeV. It is very encouraging that all of these configurations are accessible in the Groningen experiment. The NN force predictions are rather close together. Including the TM 3NF generally increases the cross section in these configurations.

Predictions based on the TM' and Urbana IX forces are of similar magnitude to the TM ones.

B. Deuteron vector analyzing power

The $A_y^{(d)}$ seems to be a good tool to investigate 3NF effects. The most sensitive configurations occur where the energies of two outgoing protons are small (< 35 MeV). Unfortunately due to the experimental arrangement, which allows to measure only protons with $E_i \geq 15$ MeV many interesting configurations will not be studied in the experiment. Nevertheless we found extended regions of the phase space with $\theta_{1,2} \geq 20^\circ$ and $\phi_{12} \leq 50^\circ$ where the value of $\delta A_y^{(d)}$ reaches more than 60%. From these regions we picked a few configurations and show them in Fig. 19. The “2N” and “2N+TM” bands are well separated showing clear and large (up to 70%) 3NF effects. The NN force band is rather narrow, whereas the “2N+TM” band is distinctly broader. For the chosen configurations the CD Bonn+TM' and AV18+Urbana IX are close to each other and predict very small 3NF effects, different from that of the TM 3NF.

C. Tensor analyzing powers

Finally, we consider the three tensor analyzing powers A_{xx} , A_{yy} and A_{xz} . The effects in A_{xx} strongly depend on the energy and, unfortunately, the most interesting part of the phase space with largest effects is outside the range of the Groningen experiment ($E_{1,2} \leq 15$ MeV and $\theta_{1,2} \geq 40^\circ$). However, we found some regions where smaller but clear 3NF effects are visible (see Fig. 20). The predictions obtained using Urbana IX and TM' forces are close together and often they do not differ from the pure NN force predictions.

For A_{yy} we found that the most sensitive parts of the accessible phase space are for $20^\circ \leq \theta_1 \leq 25^\circ$ and $\theta_2 \leq 25^\circ$ with $\phi_{12} \leq 60^\circ$. In Fig. 21 we show the three most interesting configurations. The “2N” and “2N+TM” bands are rather narrow and large 3NF effects rising above 100% are clearly visible. The Urbana IX and TM' predictions are rather close together and give smaller effects than the TM 3NF.

For A_{xz} the configurations with largest effects are for $\theta_{1,2} \cong 20^\circ$ and $\phi_{12} \geq 130^\circ$. These configurations correspond to the situation where the energy of one of the outgoing nucleons is much larger than the energy of the other nucleon. In Fig. 22 we show three examples where the 3NF effects are larger than 100%. Again the effects of Urbana IX and TM' are significantly smaller than the effects of TM 3NF.

In conclusion, in the $\vec{d}\vec{N}$ breakup reaction with an incoming deuteron energy of 130 MeV the 3NF effects are clearly visible for cross section, vector and tensor analyzing powers in numerous configurations. The most promising observables are the tensor analyzing powers where the 3NF effects are as large as 100-180%. For these observables the magnitudes of the effects depend on the 3NF model used.

V. SUMMARY AND CONCLUSIONS

We started our investigation with the nd total cross section. As could be foreseen we found that the magnitude of 3NF effects increases with energy. Because at higher energies the breakup contribution to the total nd cross section becomes dominant this implies that the breakup process should be especially gratifying to see 3NF effects. In such a process, where the three final momenta and, in addition, also some spin orientations are fixed, one has the most sensitive insight into the 3N Hamiltonian. Therefore we performed a detailed study of the nd breakup reaction focusing our investigations on the effects of 3NFs on the cross section and quite a few polarization observables. We compared predictions based on realistic NN forces (CD Bonn, AV18, Nijm I, II and 93) to those obtained when, in addition, three different 3NF models (TM, TM' and Urbana IX) were included in the 3N Hamiltonian. The NN force predictions only have a certain spread. Also adding 3NFs to them yields again a spread. We talk of 3NF effects if the two spreads are clearly distinct. We have found in cross sections and analyzing powers large 3NF effects which clearly should be discernible by experiments.

In our study we covered the entire phase space at several energies: 13, 65, 135 and 200 MeV. We located for each observable the regions in phase space where the largest 3NF effects occur. These regions are in general different for the various observables. The 3NF effects increase in general with energy. Especially promising will be the tensor analyzing powers A_{xx} , A_{yy} and A_{xz} . Also the five-fold differential cross section turned out to be a promising observable to clearly see 3NF effects. The smallest effects have been found for the analyzing powers A_x and A_z . We did not study all possible force combinations between the five high precision NN forces and the three 3NF models, which are currently most often used. Our study aimed only at a first orientation. But the results show that the outcome for the 3NF effects can depend very much on the force combination. This tells that the 3NF effects predicted should be considered with some caution. All the forces are still widely based on phenomenology. Nevertheless the results indicate that very likely the effects will not be distributed rather smoothly over the whole phase space but the large effects will be concentrated in special regions. Our study might therefore help to guide future experimental searches.

As an example of such guidance we performed calculations for the $p(\vec{d}, pp)n$ experiment currently under way at KVI Groningen. This experiment covers a good fraction of the full phase space. It will be very interesting to see how the upcoming data for cross section, vector and tensor analyzing powers will be related to our predictions.

We have just begun to understand the role which 3NFs play in a nuclear Hamiltonian. Our present study, though not complete, clearly shows the significance and importance of the 3NF effects in the breakup process, especially at higher energies. A natural extension of this study is the four-nucleon scattering that might reveal even more sensitivity to the underlying forces. The first steps toward that goal have already been made [70–72].

In order to fully understand the Nd scattering dynamics at higher energies it is necessary, in addition to the inclusion of 3NFs, to formulate the equations in a relativistically covariant way. Also exact inclusion of the pp Coulomb force in pd scattering at energies above the deuteron breakup threshold is still unsolved and leaves a very uncomfortable theoretical uncertainty in the analysis of pd data. The solution of these two problems: the relativistic

formulation of 3N scattering equations and the exact inclusion of the Coulomb interactions above the deuteron breakup threshold will remove the remaining uncertainties and will make Nd scattering an extremely precise tool for testing nuclear interactions. It will also allow to compute exact 3N wave functions that can be used to study electromagnetic processes in the 3N system for a wide range of energies.

ACKNOWLEDGMENTS

This work was supported by the Polish Committee for Scientific Research (Grant No. 2P03B02818 and 5P03B12320), the Deutsche Forschungsgemeinschaft (J.G.), and the NSF (Grant No. PHY0070858). One of us (W.G.) would like to thank the Foundation for Polish Science for the financial support during his stay in Cracow. R.S. is a holder of scholarship from the Foundation for Polish Science and acknowledges financial support. The numerical calculations have been performed on the Cray T90 and T3E of the NIC in Jülich, Germany.

REFERENCES

- [1] W. Meier, W. Glöckle, Phys. Lett. **B138**, 329 (1984); B. H. J. McKeller, W. Glöckle, Nucl. Phys. **A416**, 435 (1984).
- [2] Proceedings of the International Symposium on the Three-Body Force in the Three-Nucleon System, Washington D.C., April, 1986, Eds. B. L. Berman, B. F. Gibson, Lecture Notes in Physics 260 (1986).
- [3] W. Glöckle, H. Witała, D. Hüber, H. Kamada and J. Golak, Phys. Rep. **274**, 107 (1996).
- [4] V. G. J. Stoks, R. A. M. Klomp, C. P. F. Terheggen, J. J. de Swart, Phys. Rev. **C49**, 2950 (1994).
- [5] R. B. Wiringa, V. G. J. Stoks, R. Schiavilla, Phys. Rev. **C51**, 38 (1995).
- [6] R. Machleidt, F. Sammarruca, and Y. Song, Phys. Rev. **C53**, R1483 (1996).
- [7] R. Machleidt, Phys. Rev. **C63**, 024001 (2001).
- [8] S. Weinberg, Phys. Lett. **B251**, 288 (1990); Nucl. Phys. **B363**, 3 (1991).
- [9] U. van Kolck, Phys. Rev. **C49**, 2932 (1994).
- [10] C. Ordoñez, L. Ray, U. van Kolck, Phys. Rev. **C53**, 2086 (1996).
- [11] T.-S. Park, K. Kubodera, D.-P. Min, M. Rho, Nucl. Phys. **A646**, 83 (1999).
- [12] N. Kaiser, R. Brockmann, W. Weise, Nucl. Phys. **A625**, 758 (1997).
- [13] N. Kaiser, S. Gerstendörfer, W. Weise, Nucl. Phys. **A637**, 395 (1998).
- [14] E. Epelbaum, W. Glöckle, U.-G. Meißner, Nucl. Phys. **A637**, 107 (1998).
- [15] E. Epelbaum, W. Glöckle, U.-G. Meißner, Nucl. Phys. **A671**, 295 (2000).
- [16] M. R. Robilotta, Phys. Rev. **C63**, 044004 (2001).
- [17] E. Epelbaum, H. Kamada, A. Nogga, H. Witała, W. Glöckle, U.-G. Meißner, Phys. Rev. Lett. **86**, 4787 (2001).
- [18] D. R. Entem, R. Machleidt, Phys. Lett. **B524**, 93 (2002).
- [19] E. Epelbaum *et al.*, nucl-th/0201064.
- [20] E. Epelbaum *et al.*, to appear in Proceedings of the conference on "Mesons and Light Nuclei", Prague, July 2001 (nucl-th/0109065).
- [21] D. R. Entem, R. Machleidt, H. Witała, nucl-th/0111033.
- [22] A. Nogga, H. Kamada, and W. Glöckle, Phys. Rev. Lett. **85**, 944 (2000).
- [23] M. Viviani, Nucl. Phys. **A631**, 111c (1988).
- [24] A. Nogga, H. Kamada, W. Glöckle, B.R. Barrett, nucl-th/0112026.
- [25] J. Carlson, R. Schiavilla, Rev. of Mod. Phys. **70**, 743 (1998).
- [26] R. B. Wiringa, S. C. Pieper, J. Carlson, and V. R. Pandharipande, Phys. Rev. **C62**, 014001 (2000).
- [27] J. Fujita, H. Miyazawa, Prog. Theor. Phys. **17**, 360 (1957).
- [28] B. S. Pudliner, V. R. Pandharipande, J. Carlson, S. C. Pieper, and R. B. Wiringa, Phys. Rev. **C56**, 1720 (1997).
- [29] S. A. Coon *et al.*, Nucl. Phys. **A317**, 242 (1979).
- [30] S. C. Pieper *et al.*, Phys. Rev. **C64**, 014001 (2001).
- [31] K. Sekiguchi *et al.*, Phys. Rev. **C65**, 034003 (2002).
- [32] H. O. Meyer, private communication.
- [33] K. Bodek, private communication.
- [34] K. Sagara, private communication.
- [35] H. Sakai *et al.*, Phys. Rev. Lett. **84**, 5288 (2000).
- [36] N. Sakamoto *et al.*, Phys. Lett. **B367**, 60 (1996).

- [37] W. Tornow, C. R. Howell, R. C. Byrd, R. S. Peroni, and R. L. Walter, Phys. Rev. Lett. **49**, 312 (1982).
- [38] R. V. Cadman *et al.*, Phys. Rev. Lett. **86**, 967 (2001).
- [39] R. Bieber *et al.*, Phys. Rev. Lett. **84**, 606 (2000).
- [40] K. Ermisch *et al.*, Phys. Rev. Lett. **86**, 5862 (2001).
- [41] P. Hепен *et al.*, Phys. Rev. **C57**, 484 (1998).
- [42] W. Grüebler *et al.*, Nucl. Phys. **A353**, 31c (1981).
- [43] L. Sydow *et al.*, Nucl. Phys. **A567**, 55 (1994); L. Sydow *et al.*, Few-Body Syst. **25**, 133 (1998).
- [44] H. Witała *et al.*, Phys. Rev. **C63**, 024007 (2001).
- [45] St. Kistryn *et al.*, Nucl. Phys. **A689**, 345c (2001).
- [46] D. Hüber, H. Kamada, H. Witała, and W. Glöckle, Acta Physica Polonica **B28**, 1677 (1997).
- [47] A. Stadler, W. Glöckle, P. U. Sauer, Phys. Rev. **C44**, 2319 (1991).
- [48] G. O. Ohlsen, Rep. Prog. Phys. **35** (1972) 717.
- [49] G. G. Ohlsen, R. E. Brown, F. D. Correll, and R. A. Hardekopf, Nucl. Instr. and Methods **179**, 283 (1981).
- [50] S. A. Coon, W. Glöckle, Phys. Rev. **C23**, 1790 (1981).
- [51] S. A. Coon, H. P. Han, Few-Body Syst. **30**, 131 (2001).
- [52] For a short review see M. R. Robilotta, Few-Body Syst. **Suppl. 2**, 35 (1987).
- [53] S. A. Coon, M. T. Peña, Phys. Rev. **C48**, 2559 (1993).
- [54] S. A. Coon, M. T. Peña, D. O. Riska, Phys. Rev. **C52**, 2925 (1995).
- [55] B. D. Keister, R. B. Wiringa, Phys. Lett. **B173**, 5 (1986).
- [56] T.-Y. Saito, J. Haidenbauer, nucl-th/0003064.
- [57] H. Witała *et al.*, Phys. Rev. **C52**, 1254 (1995).
- [58] J. L. Friar, D. Hüber, U. van Kolck, Phys. Rev. **C59**, 53 (1999).
- [59] D. Hüber, J. L. Friar, A. Nogga, H. Witała, U. van Kolck, Few-Body Syst. **30**, 95 (2001).
- [60] M. R. Robilotta, H. T. Coelho, Nucl. Phys. **A460**, 645 (1986).
- [61] A. Kievsky, M. Viviani, and S. Rosati, Phys. Rev. **C52**, R15 (1995).
- [62] J. Carlson, V. R. Pandharipande, R. B. Wiringa, Nucl. Phys. **A401**, 59 (1983).
- [63] H. Witała, W. Glöckle, J. Golak, D. Hüber, H. Kamada, and A. Nogga, Phys. Lett. **B 447**, 216 (1999).
- [64] P. U. Sauer, Prog. Part. Nucl. Phys. **16**, 35 (1986).
- [65] S. Nemoto *et al.*, Phys. Rev. **C58**, 2599 (1999).
- [66] A. Nogga, D. Hüber, H. Kamada, and W. Glöckle, Phys. Lett. **B 409**, 19 (1997).
- [67] W. P. Abfalterer, *et al.* Phys. Rev. Lett. **81**, 57 (1998).
- [68] H. Witała *et al.*, Phys. Rev. **C59**, 3035 (1999).
- [69] J. Kuroś-Żolnierczuk, PhD thesis, Kraków, 2001,
<http://zfej-www.if.uj.edu.pl/prj/thfewbod.htm>
- [70] M. Viviani, S. Rosati, and A. Kievsky, Phys. Rev. Lett. **81**, 1580 (1998).
- [71] A. Fonseca, Phys. Rev. Lett. **83**, 4021 (1999).
- [72] F. Ciesielski, J. Carbonell, and C. Gignoux, Phys. Lett. **B447**, 199 (1999).
- [73] J. Seagrave *et al.*, Ann. Phys. (N.Y.) **74**, 250 (1972).
- [74] G. Pauletta and F. Brooks, Nucl. Phys. **A255**, 267 (1975).
- [75] M. Holmberg, Nucl. Phys. **A129**, 327 (1969).

[76] H. Catron *et al.*, Phys. Rev. **123**, 218 (1961).

TABLES

TABLE I. Comparison of the nd total breakup cross section σ_{tot}^{br} with the value σ_{tot}^{scan} evaluated according to Eq.(11) at four energies of the incoming nucleon.

E_{lab} [MeV]	σ_{tot}^{br} [mb]	σ_{tot}^{scan} [mb]
13	167.5	159.2
65	91.7	87.3
135	56.0	53.5
200	48.2	45.9

TABLE II. The maximal changes $\Delta O = \max[\delta O(E_1, E_2, \theta_1, \theta_2, \phi_{12})]$ due to 3NF effects for the eight studied observables. For each energy the first row, labeled all, gives ΔO without constraints, the second row, labeled σ -cut, gives ΔO under the condition $\sigma^{(2N)} \geq 0.01 \frac{mb}{sr^2 MeV}$, the third row, labelled $\sigma + E$ -cut, gives ΔO under the additional restriction that $E_{1,2} \geq 15(3)$ MeV for $E_{lab} = 65, 135, 200$ (13) MeV. The last column gives the total number of studied configurations (covering all values of ΔO).

E_{lab} [MeV]	cuts	$\Delta\sigma$ [%]	ΔA_x [%]	ΔA_z [%]	ΔA_y [%]	$\Delta A_y^{(d)}$ [%]	ΔA_{xx} [%]	ΔA_{yy} [%]	ΔA_{xz} [%]	N
13	all	10	0	0	7	10	22	32	19	6147
	σ -cut	10	0	0	7	10	22	32	19	6008
	$\sigma + E$ -cut	10	0	0	0	0	18	17	15	1532
65	all	23	110	33	182	88	188	194	211	7893
	σ -cut	23	97	33	156	88	188	194	205	7323
	$\sigma + E$ -cut	23	97	22	156	88	188	126	130	2002
135	all	98	202	99	327	289	357	281	577	8253
	σ -cut	98	93	58	269	233	351	166	195	7370
	$\sigma + E$ -cut	98	76	58	269	233	351	154	195	1028
200	all	133	251	205	418	458	580	702	677	8597
	σ -cut	115	81	60	238	368	275	443	230	6638
	$\sigma + E$ -cut	115	59	60	238	368	275	443	230	689

TABLE III. The same as in Table II for five observables in the $p(\vec{d}, pp)n$ breakup reaction at 130 MeV.

cuts	$\Delta\sigma$	$\Delta A_y^{(d)}$	ΔA_{xx}	ΔA_{yy}	ΔA_{xz}	N
all	23	85	197	181	172	970
σ -cut	23	85	197	181	172	970
$\sigma + E$ -cut	21	80	100	181	172	955

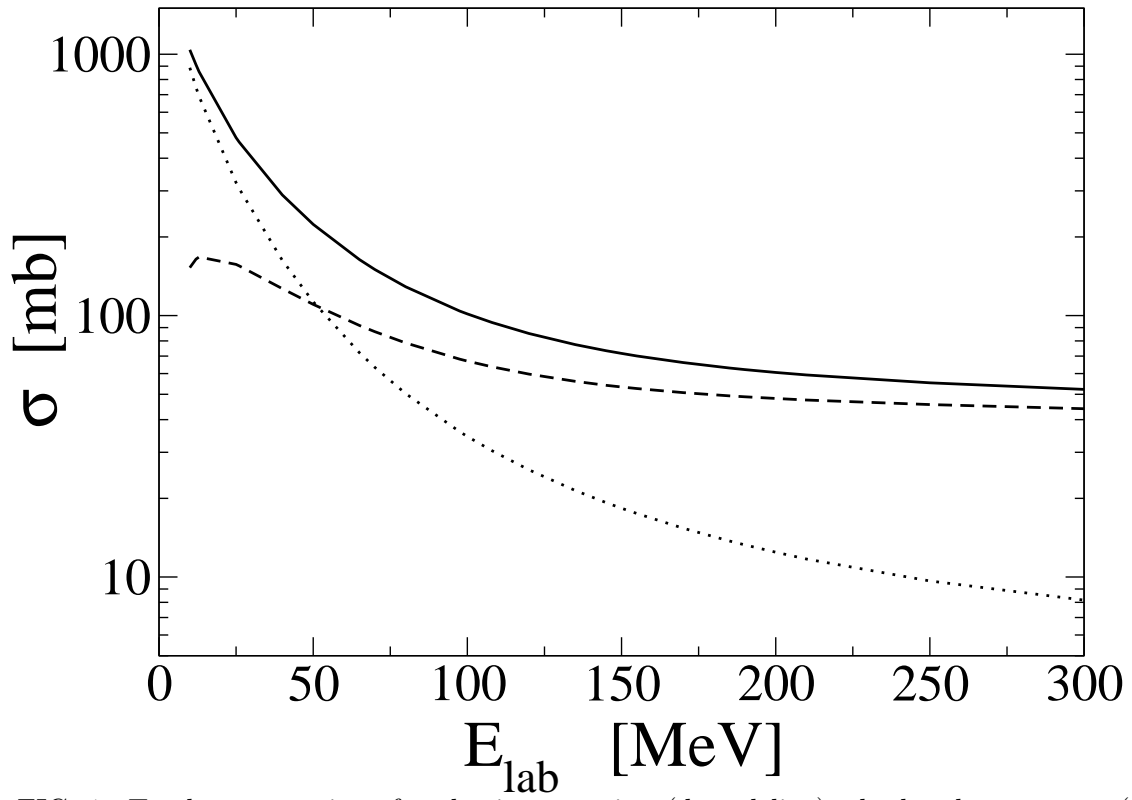


FIG. 1. Total cross sections for elastic scattering (dotted line), the breakup process (dashed line) and their sum (solid line) as predicted by the CD Bonn potential.

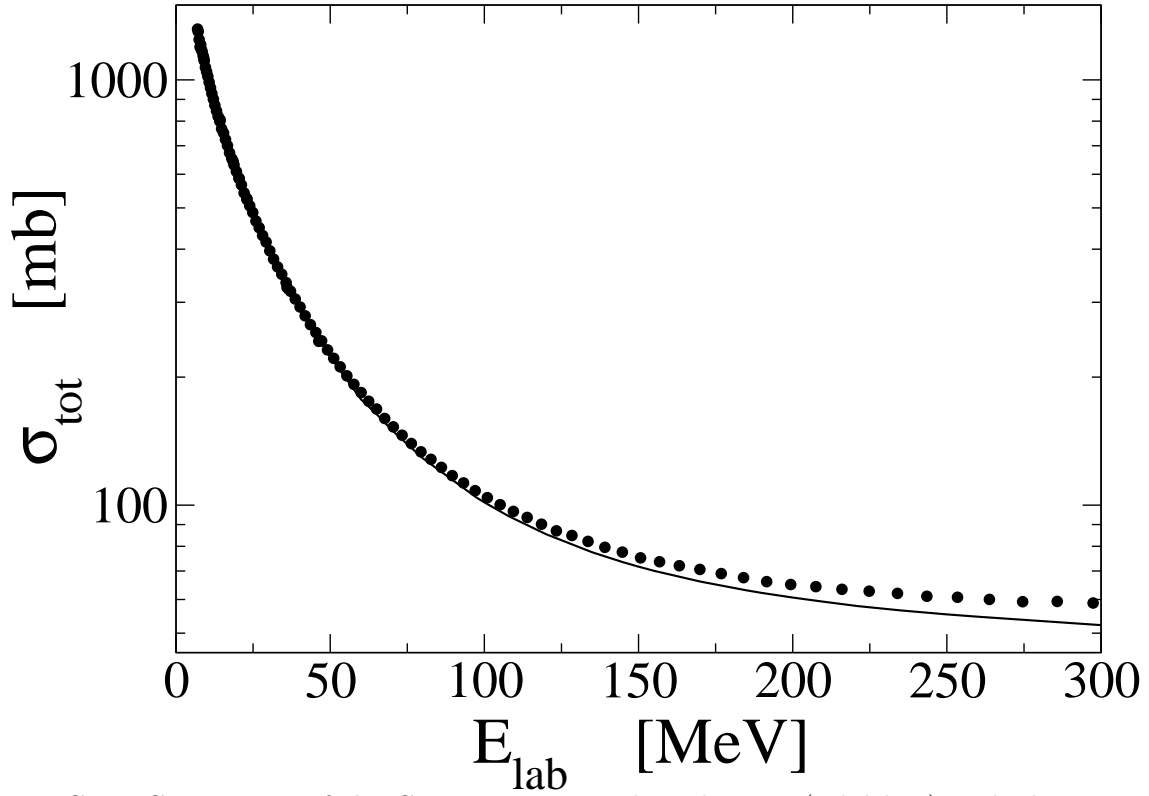


FIG. 2. Comparison of the CD Bonn potential predictions (solid line) with the experimental data (full dots) [67] for the total nd cross sections σ_{tot} .

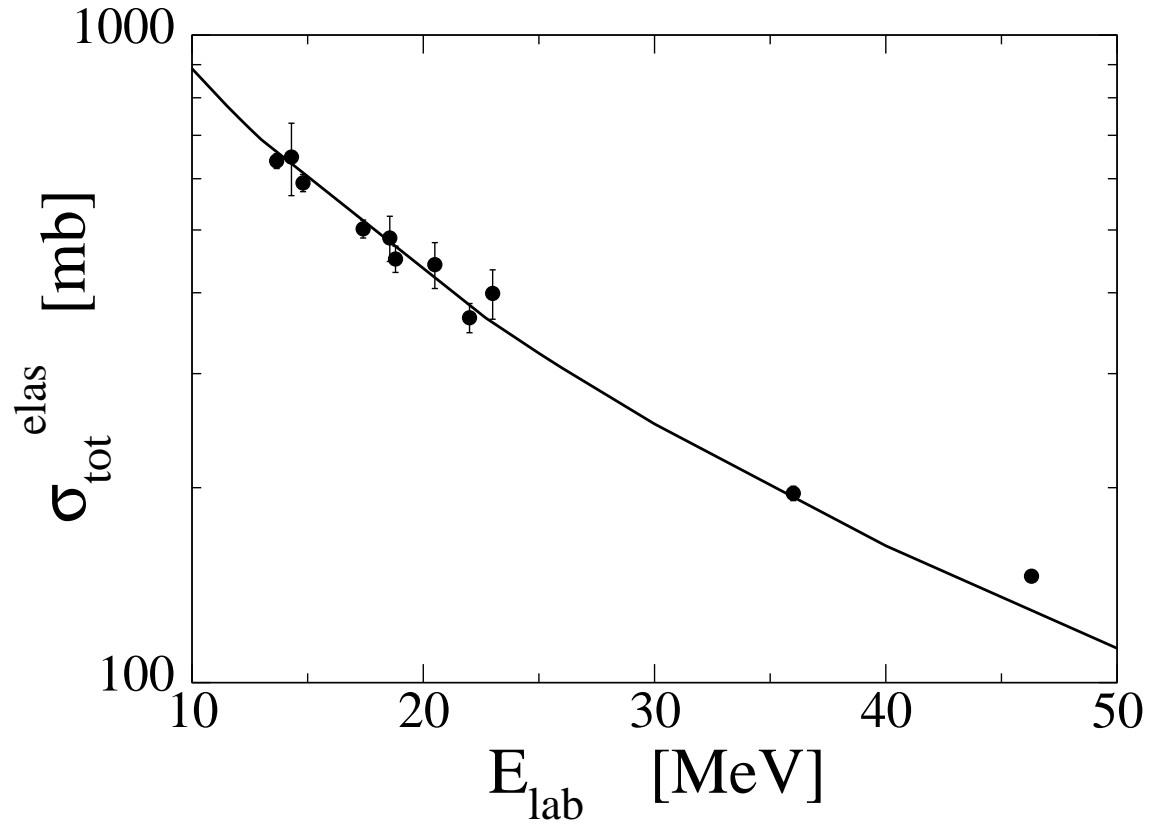


FIG. 3. Comparison of the CD Bonn potential predictions (solid line) with the experimental data (full dots) [73–76] for the total elastic cross section $\sigma_{\text{tot}}^{\text{elas}}$.

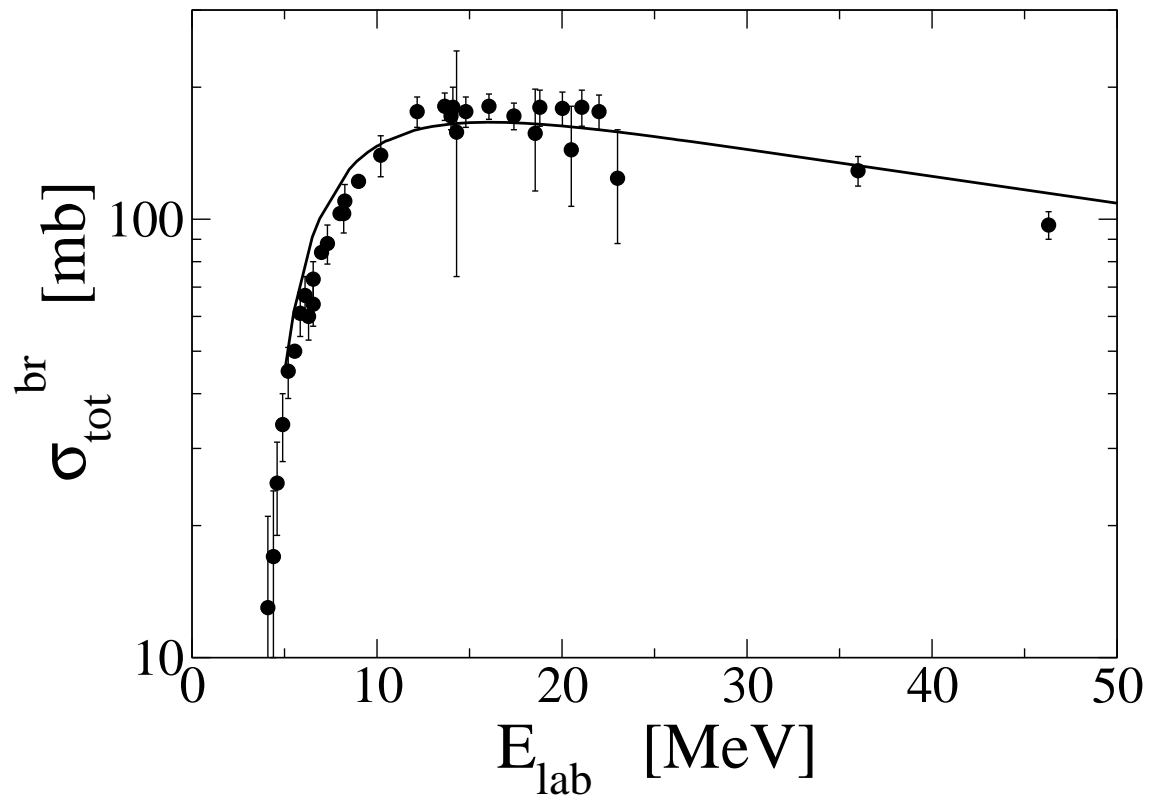


FIG. 4. Comparison of the CD Bonn potential predictions (solid line) with the experimental data (full dots) [73–76] for the total breakup cross section $\sigma_{\text{tot}}^{\text{br}}$.

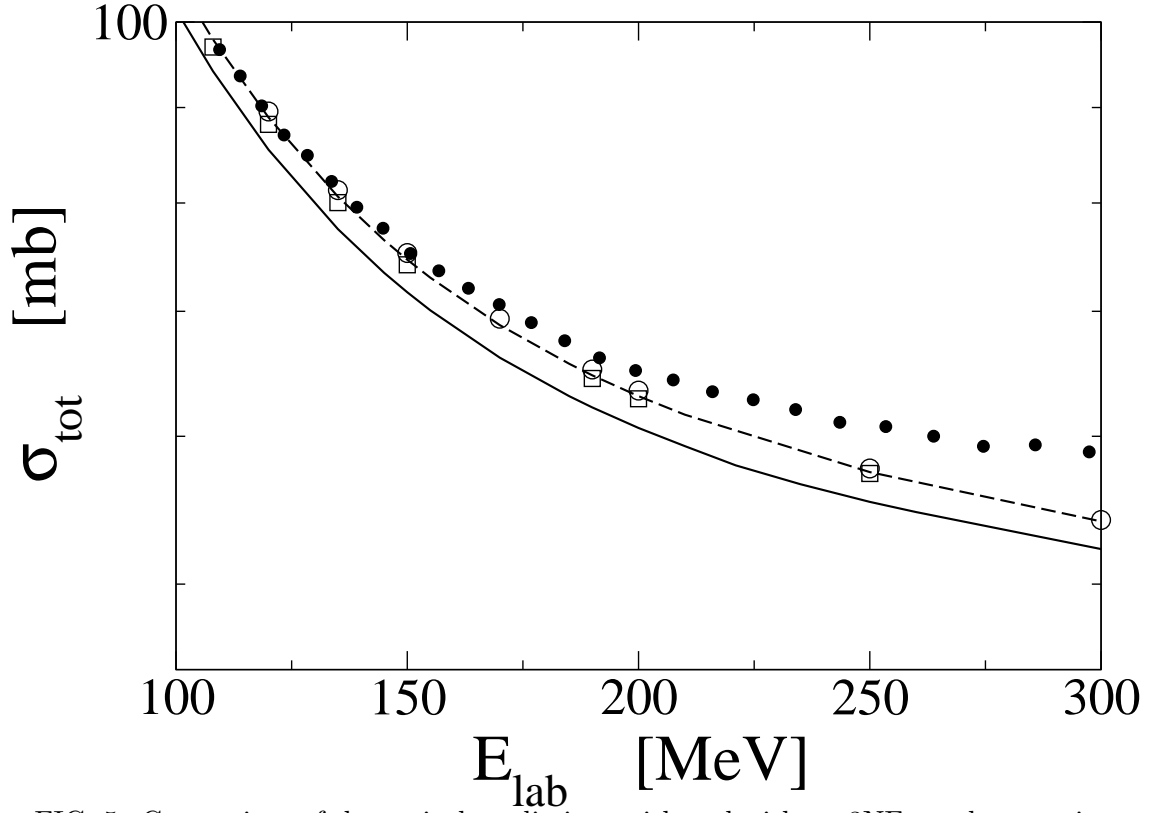


FIG. 5. Comparison of theoretical predictions with and without 3NFs to the experimental data (full dots) [67] for the nd total cross section. The solid and dashed lines are the CD Bonn and CD Bonn+TM 3NF predictions, respectively. The open squares are the results for AV18+Urbana IX and the circles for CD Bonn+TM'.

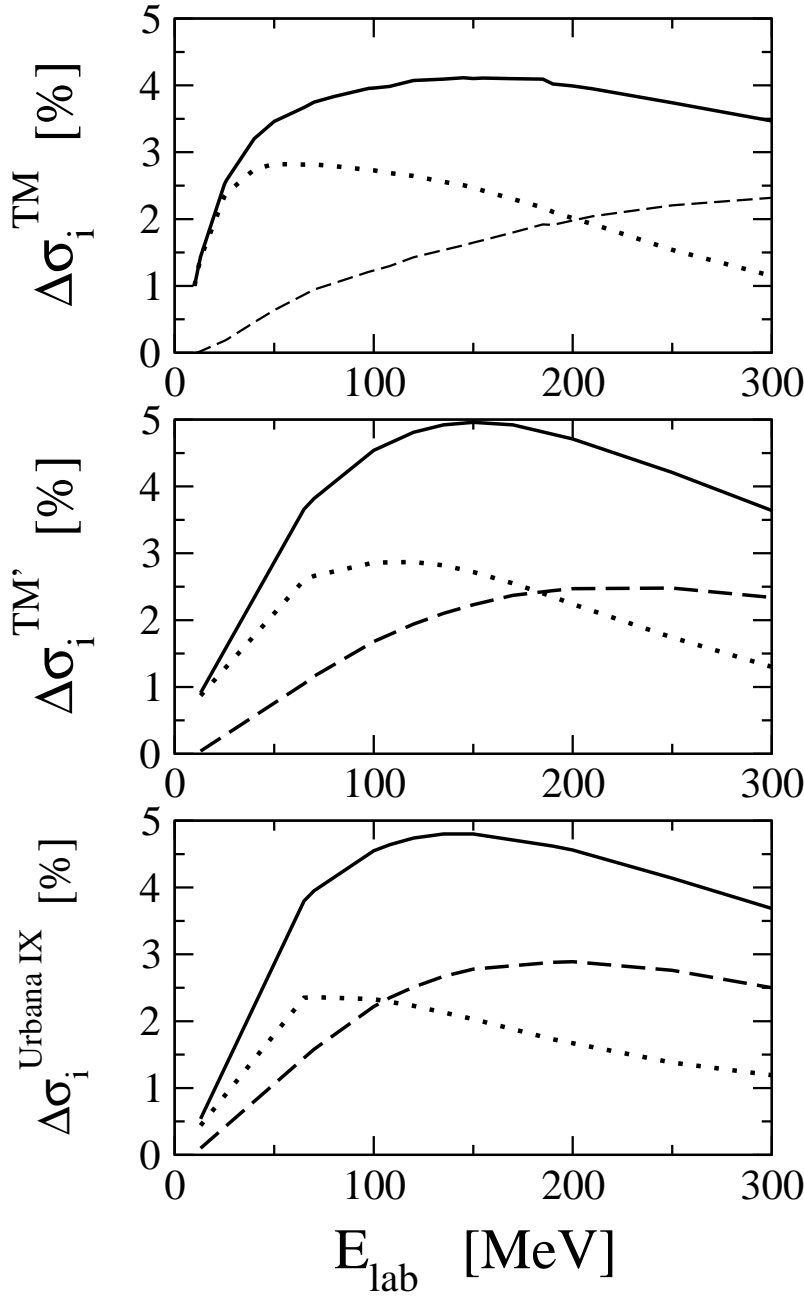


FIG. 6. 3NF effects in the nd total cross section (solid line), the total elastic scattering cross section (dotted line), and the total breakup cross section (dashed line), expressed as a percentage change (see Eq. 10) with respect to the total cross section as obtained with the NN interactions alone: CD Bonn+TM (top), CD Bonn+TM' (middle), and AV18+Urbana IX (bottom).

FIG. 7. Two-dimensional projections of phase space regions for $\Delta\sigma$ in the Nd breakup at 135 MeV. In the first row (all) phase space points are plotted without any restrictions, in the second row (σ -cut), and the third row ($\sigma + E$ -cut) the remaining points are plotted after the corresponding cuts have been performed. The three columns show the $\theta_1 - \theta_2$, $\theta_1 - \phi_{12}$ and $E_1 - E_2$ planes, respectively. The different colours express the $\Delta\sigma$ values in percentage.

FIG. 8. Two-dimensional projections of phase space regions for ΔA_{yy} in the Nd breakup at 135 MeV. For the description see caption of Fig. 7.

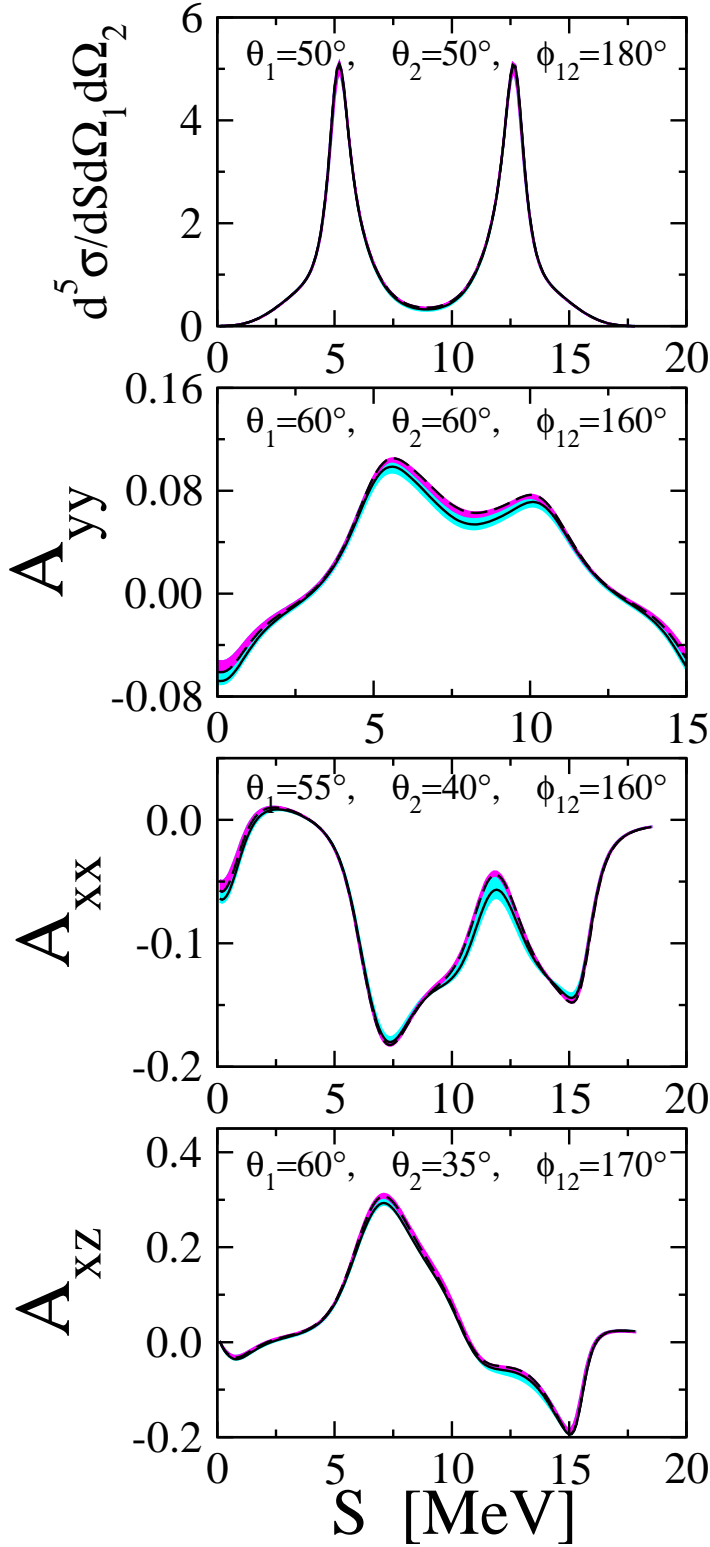


FIG. 9. Cross section in [mb MeV⁻¹sr⁻²] and analyzing powers for selected breakup configurations at 13 MeV. The light shaded band (blue) contains the theoretical predictions based on CD Bonn, AV18, Nijm I, II and Nijm 93. The darker band (red) represents predictions when these NN forces are combined with the TM 3NF. The solid line is for AV18+Urbana IX and the dashed line for CD Bonn+TM'.

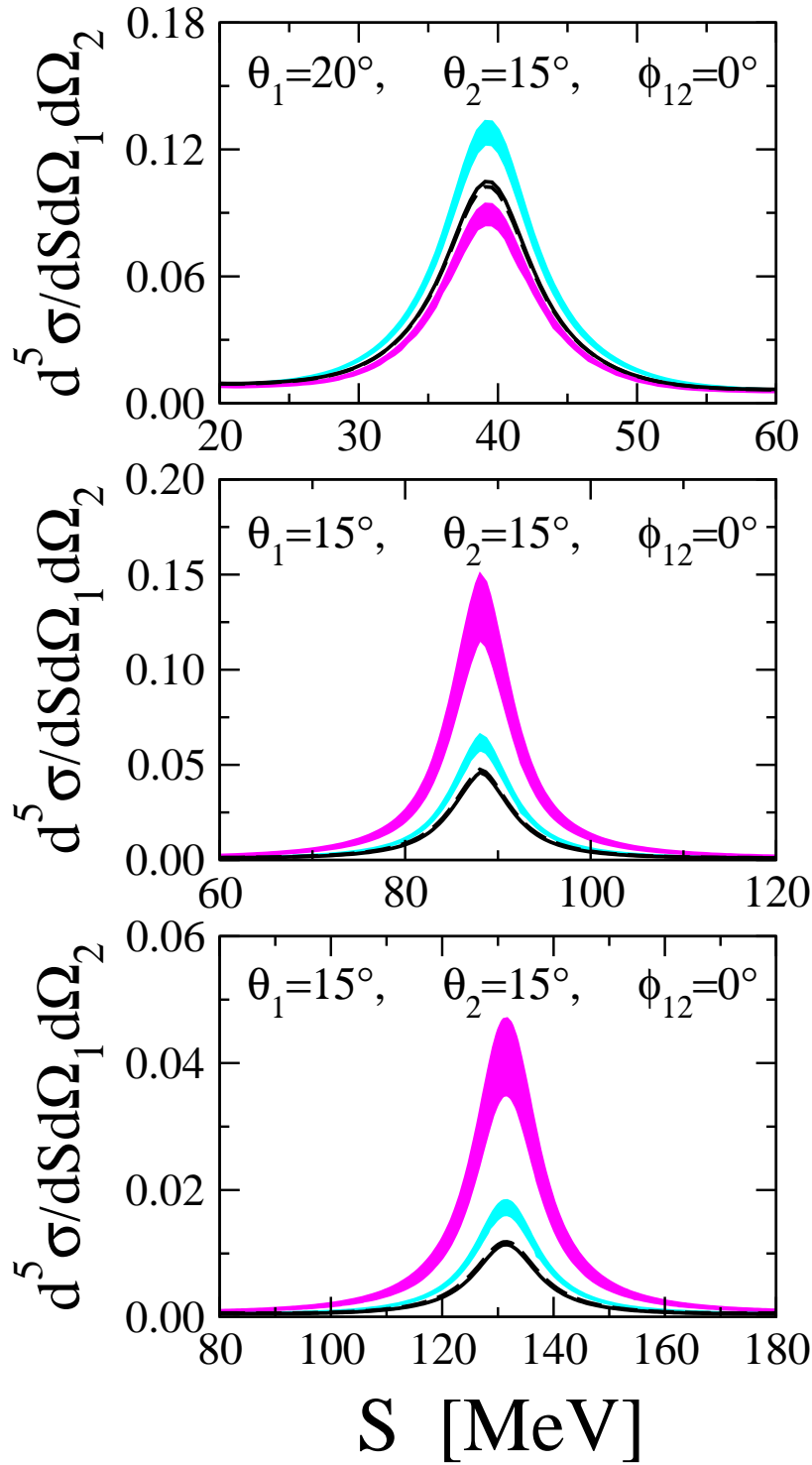


FIG. 10. Differential cross section in [mb MeV⁻¹sr⁻²] in selected breakup configurations at 65 (top), 135 (middle) and 200 MeV (bottom). For the description of bands and lines see caption of Fig. 9.

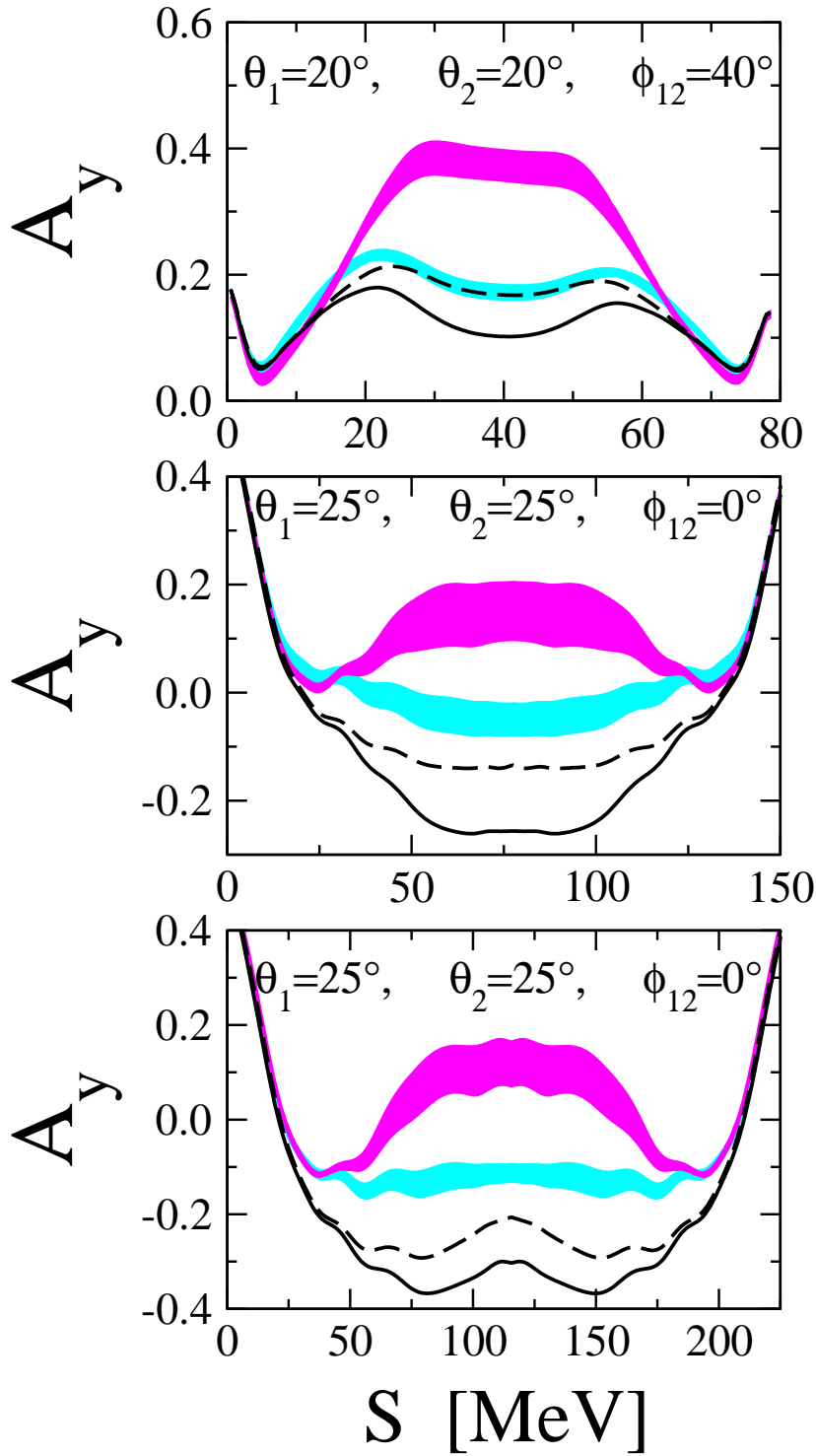


FIG. 11. Nucleon analyzing power A_y in selected breakup configurations at 65 (top), 135 (middle) and 200 MeV (bottom). For the description of bands and lines see caption of Fig. 9.

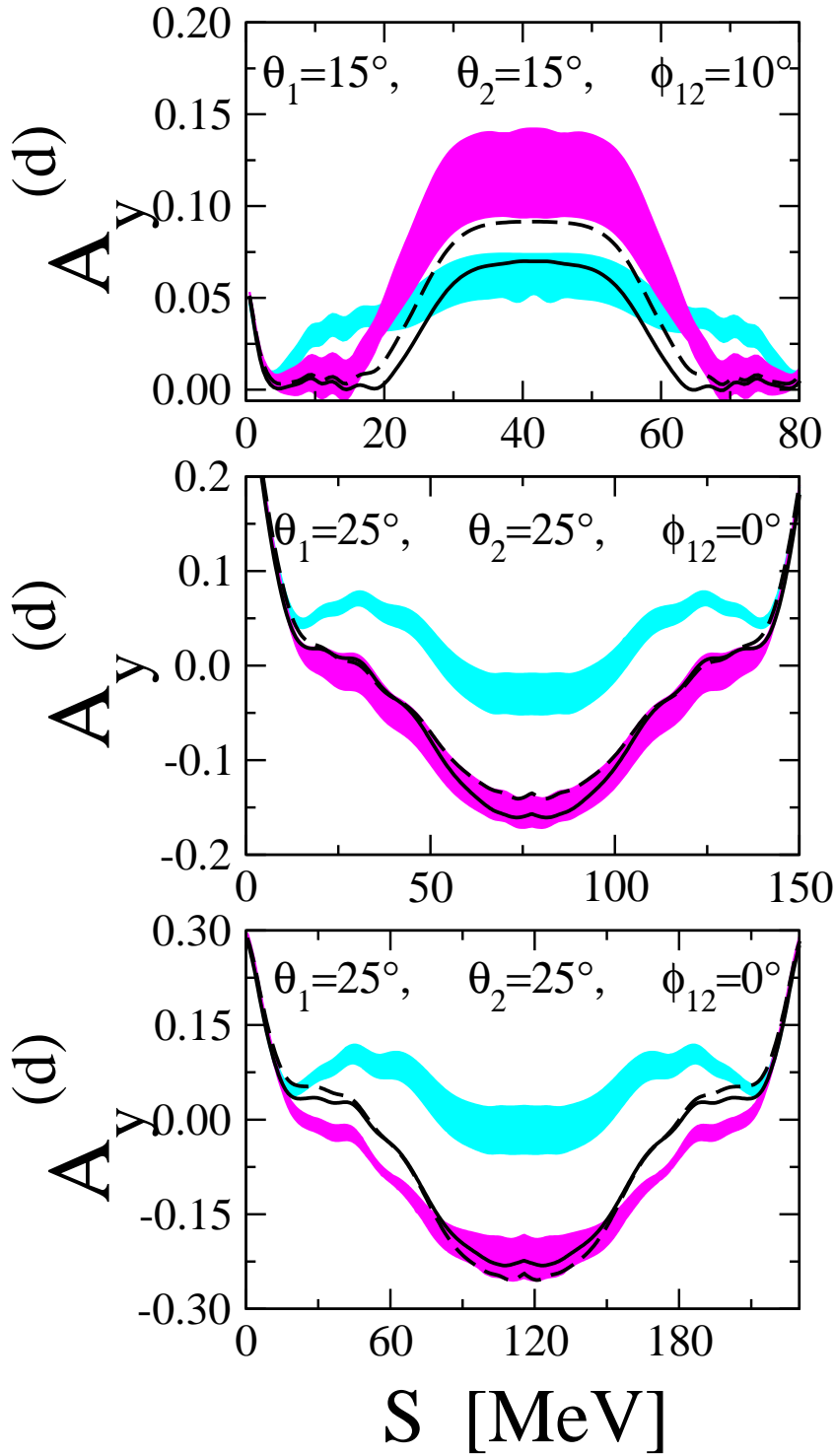


FIG. 12. Deuteron vector analyzing power $A_y^{(d)}$ in selected breakup configurations at 65 (top), 135 (middle) and 200 MeV (bottom). For the description of bands and lines see caption of Fig. 9.

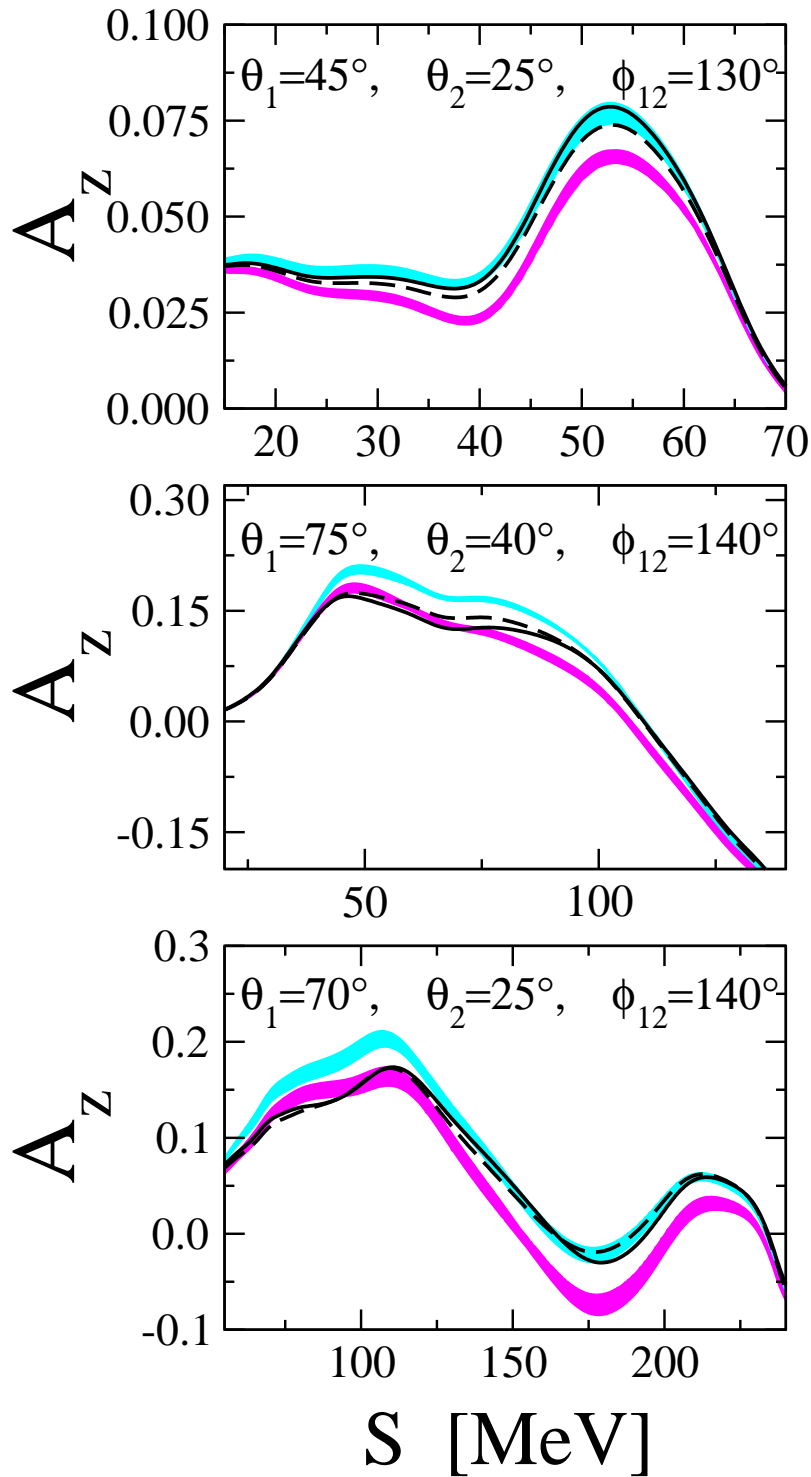


FIG. 13. Nucleon analyzing power A_z in selected breakup configurations at 65 (top), 135 (middle) and 200 MeV (bottom). For the description of bands and lines see caption of Fig. 9.

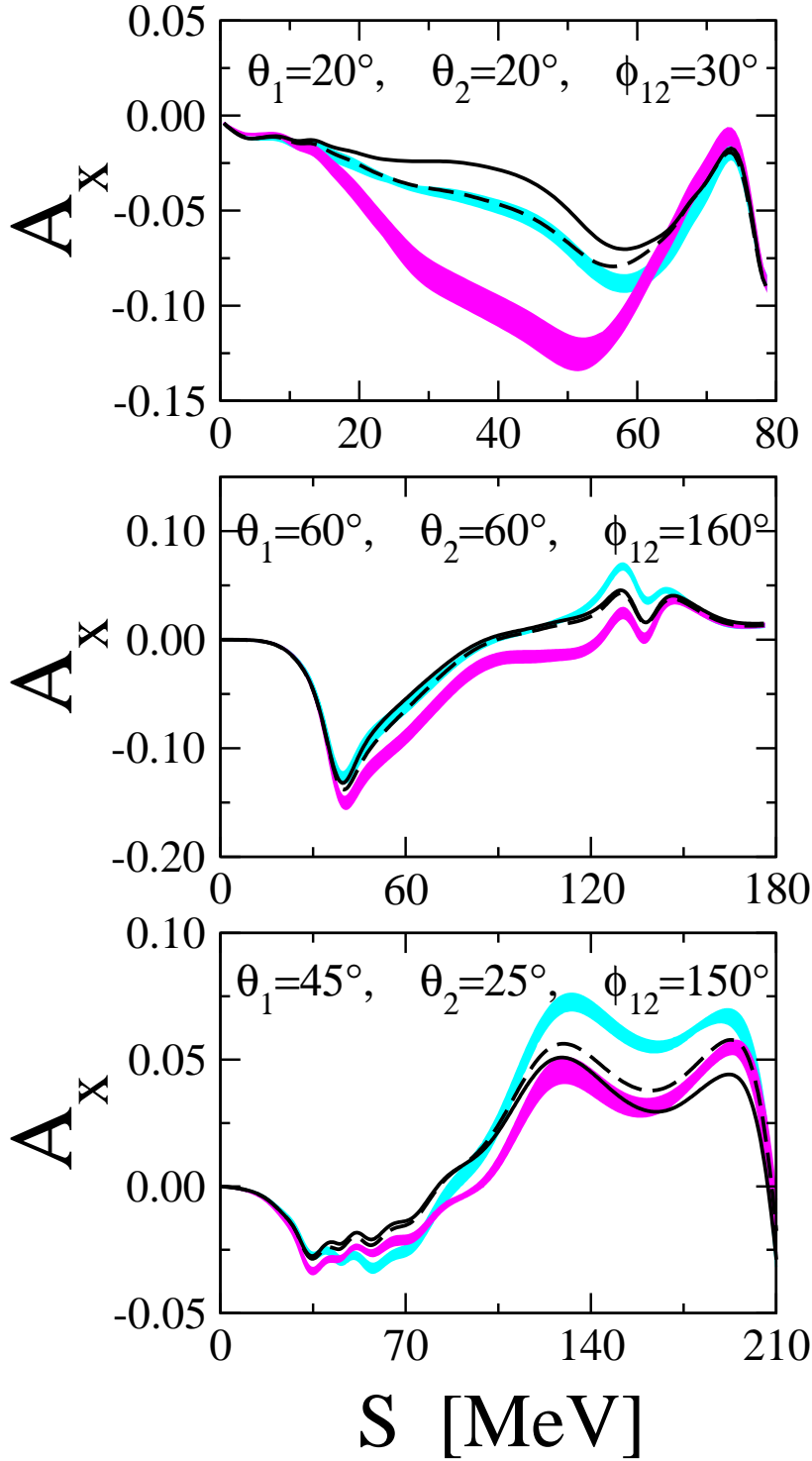


FIG. 14. Nucleon analyzing power A_x in selected breakup configurations at 65 (top), 135 (middle) and 200 MeV (bottom). For the description of bands and lines see caption of Fig. 9.

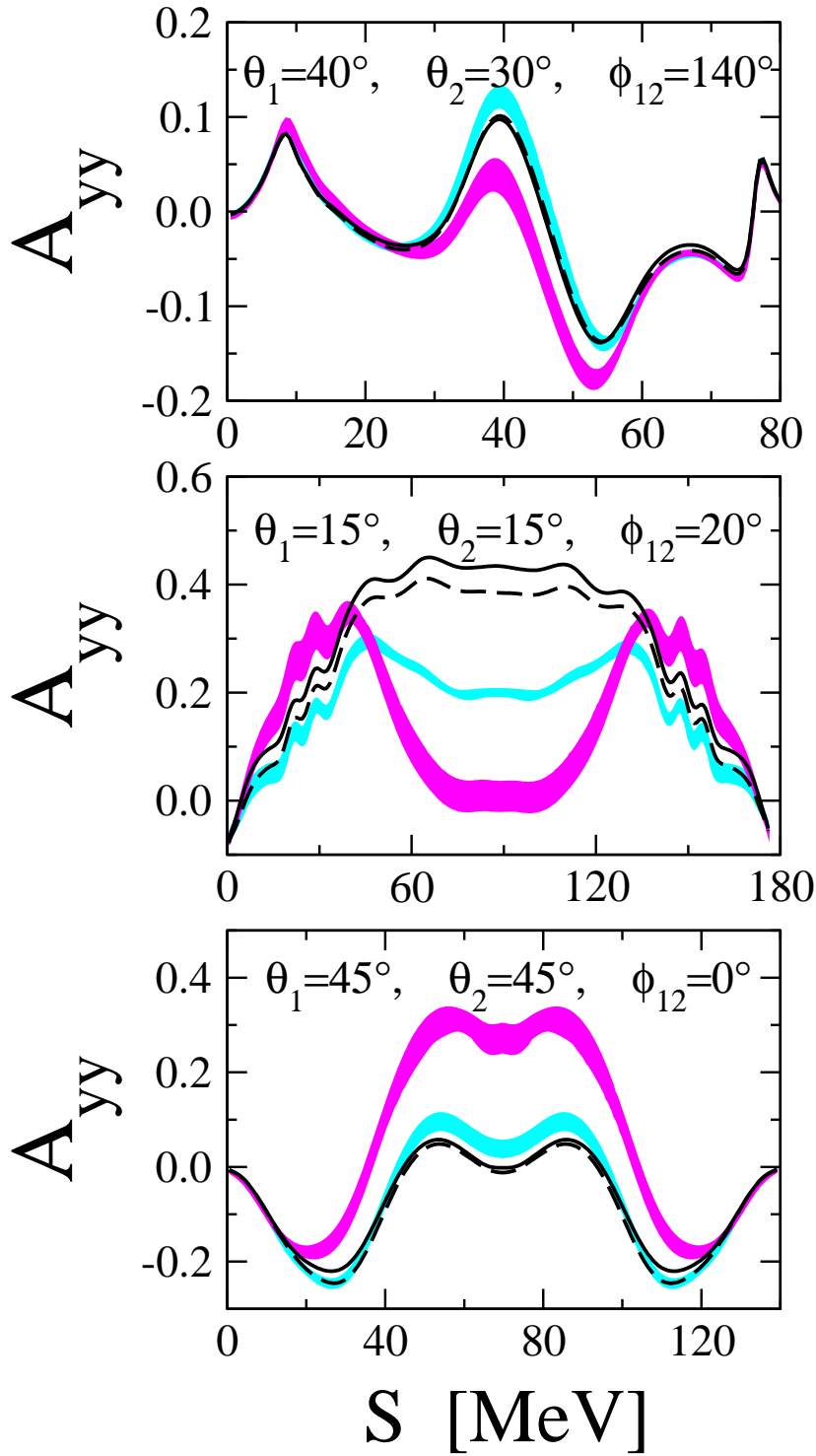


FIG. 15. Tensor analyzing power A_{yy} in selected breakup configurations at 65 (top), 135 (middle) and 200 MeV (bottom). For the description of bands and lines see caption of Fig. 9.

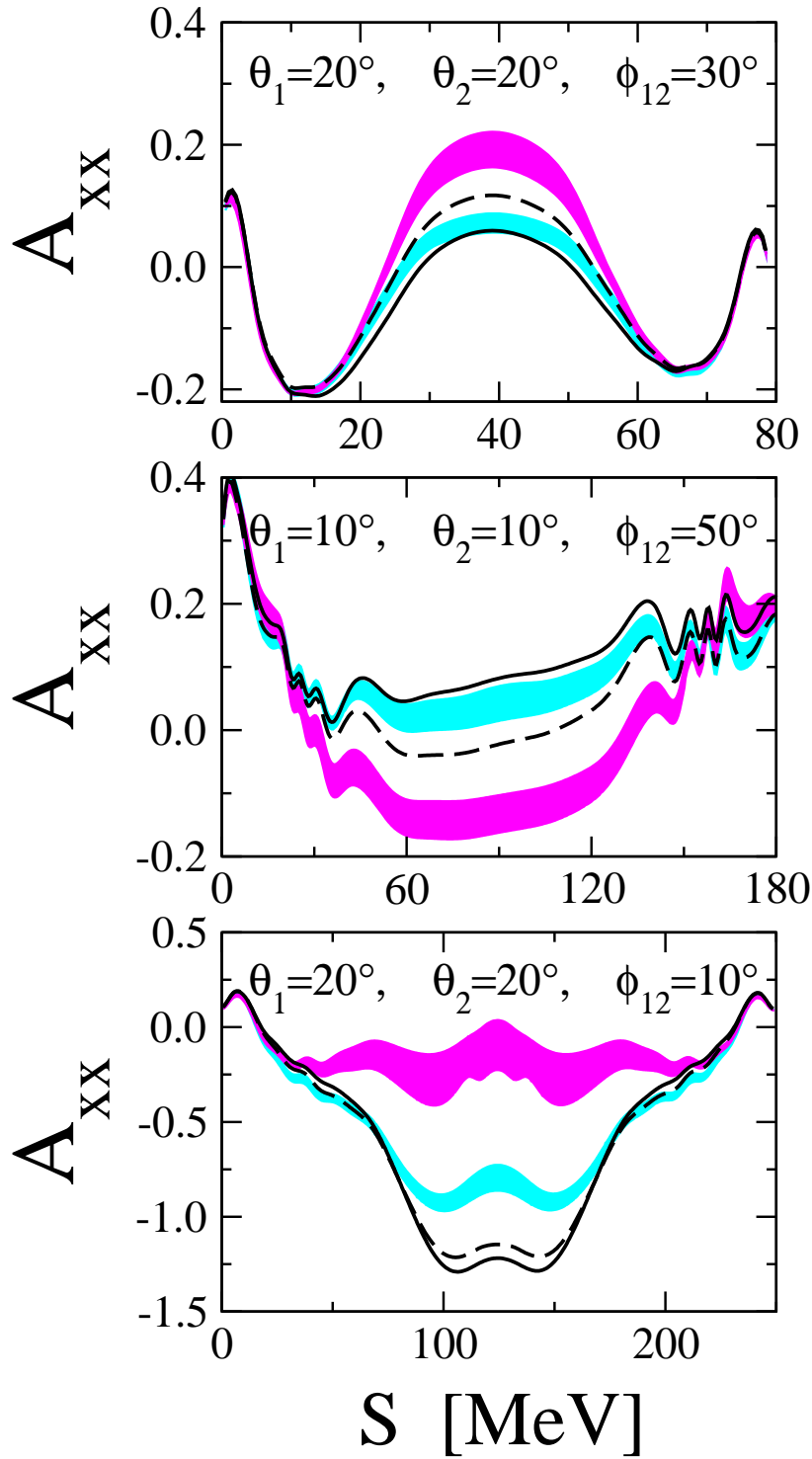


FIG. 16. Tensor analyzing power A_{xx} in selected breakup configurations at 65 (top), 135 (middle) and 200 MeV (bottom). For the description of bands and lines see caption of Fig. 9.

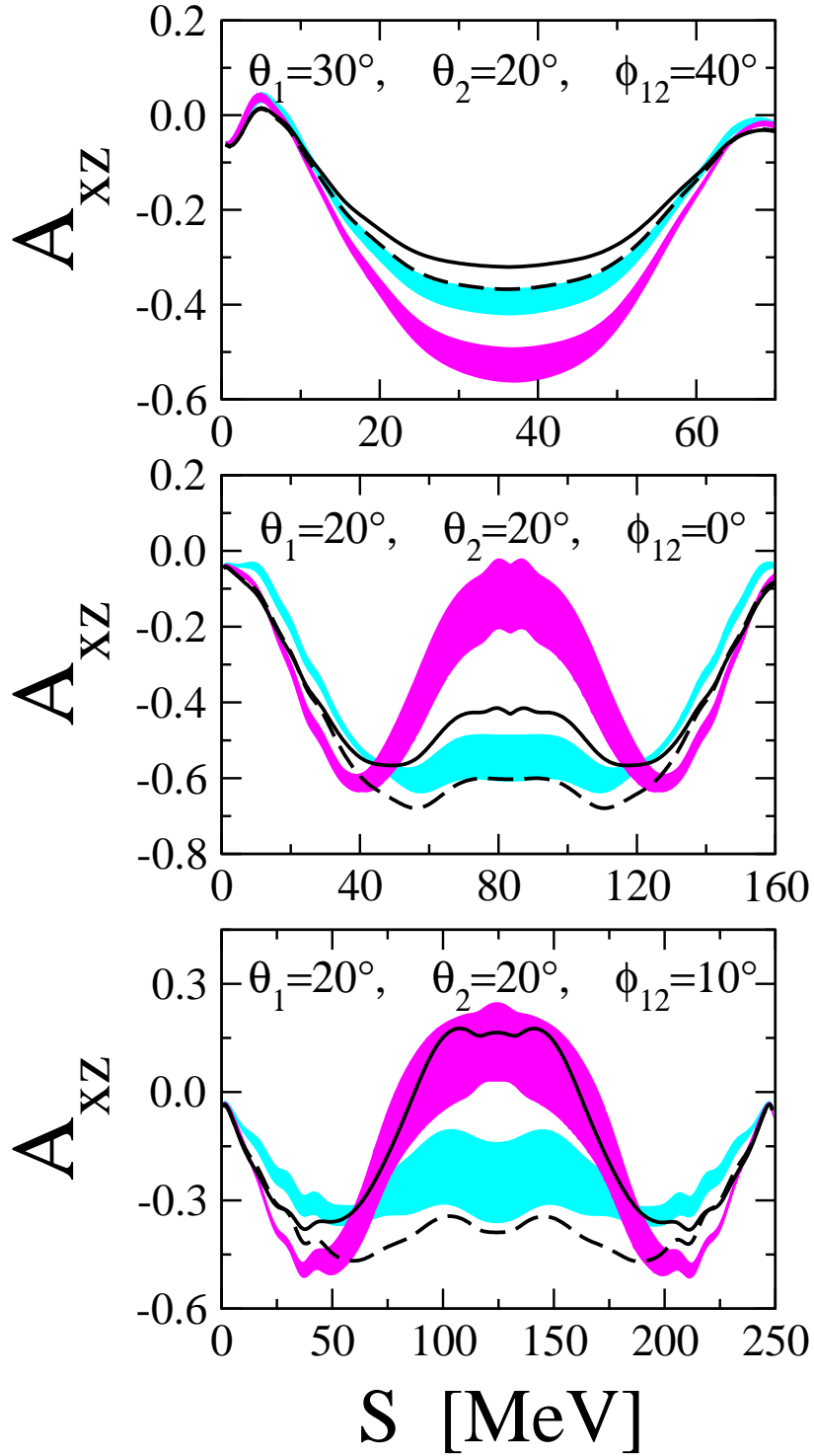


FIG. 17. Tensor analyzing power A_{xz} in selected breakup configurations at 65 (top), 135 (middle) and 200 MeV (bottom). For the description of bands and lines see caption of Fig. 9.

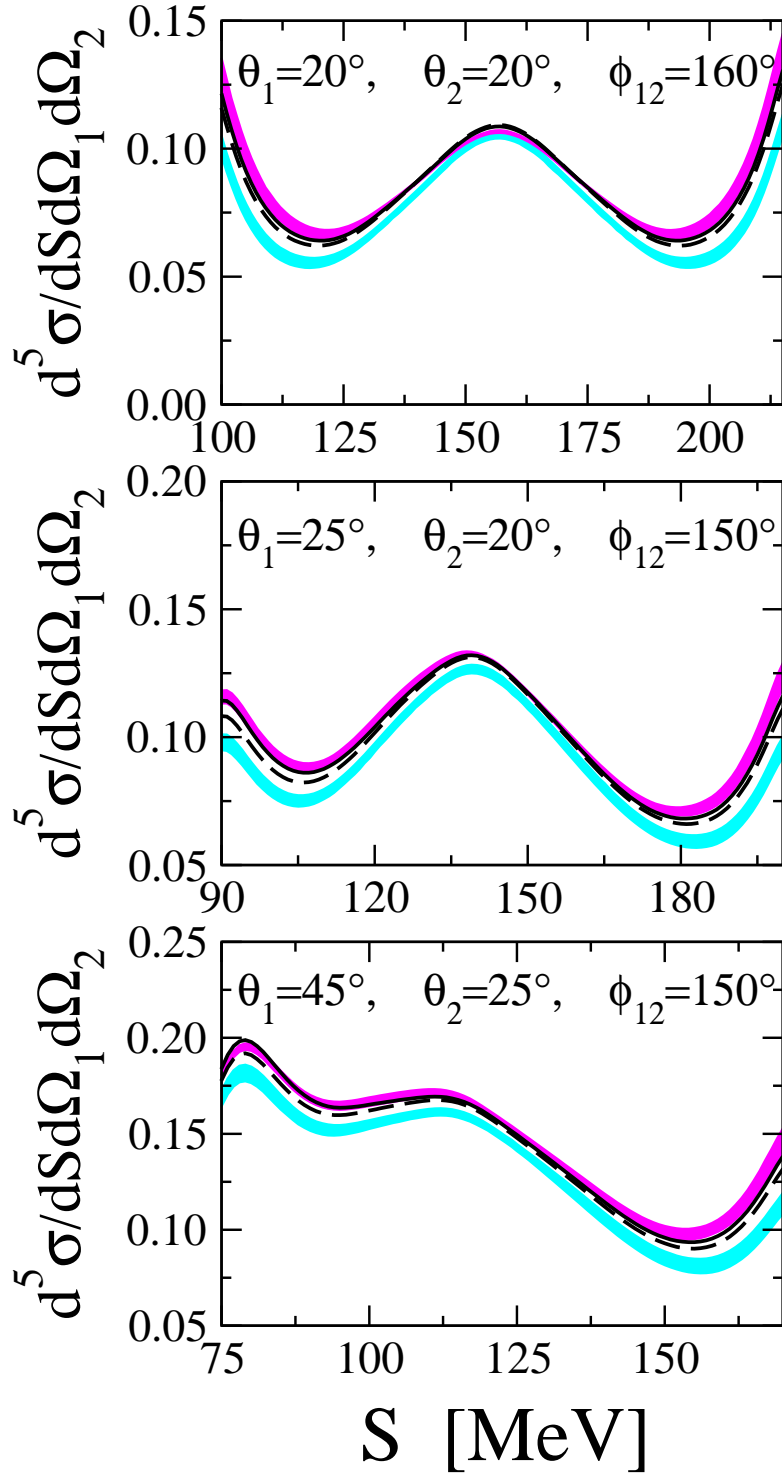


FIG. 18. Theoretical predictions for the cross section in $[\text{mb MeV}^{-1}\text{sr}^{-2}]$ of the dN breakup at 130 MeV for selected configurations. For the description of bands and lines see caption of Fig. 9. The points along the S -curve displayed in the figures correspond to the ones accessible in the Groningen experiment.

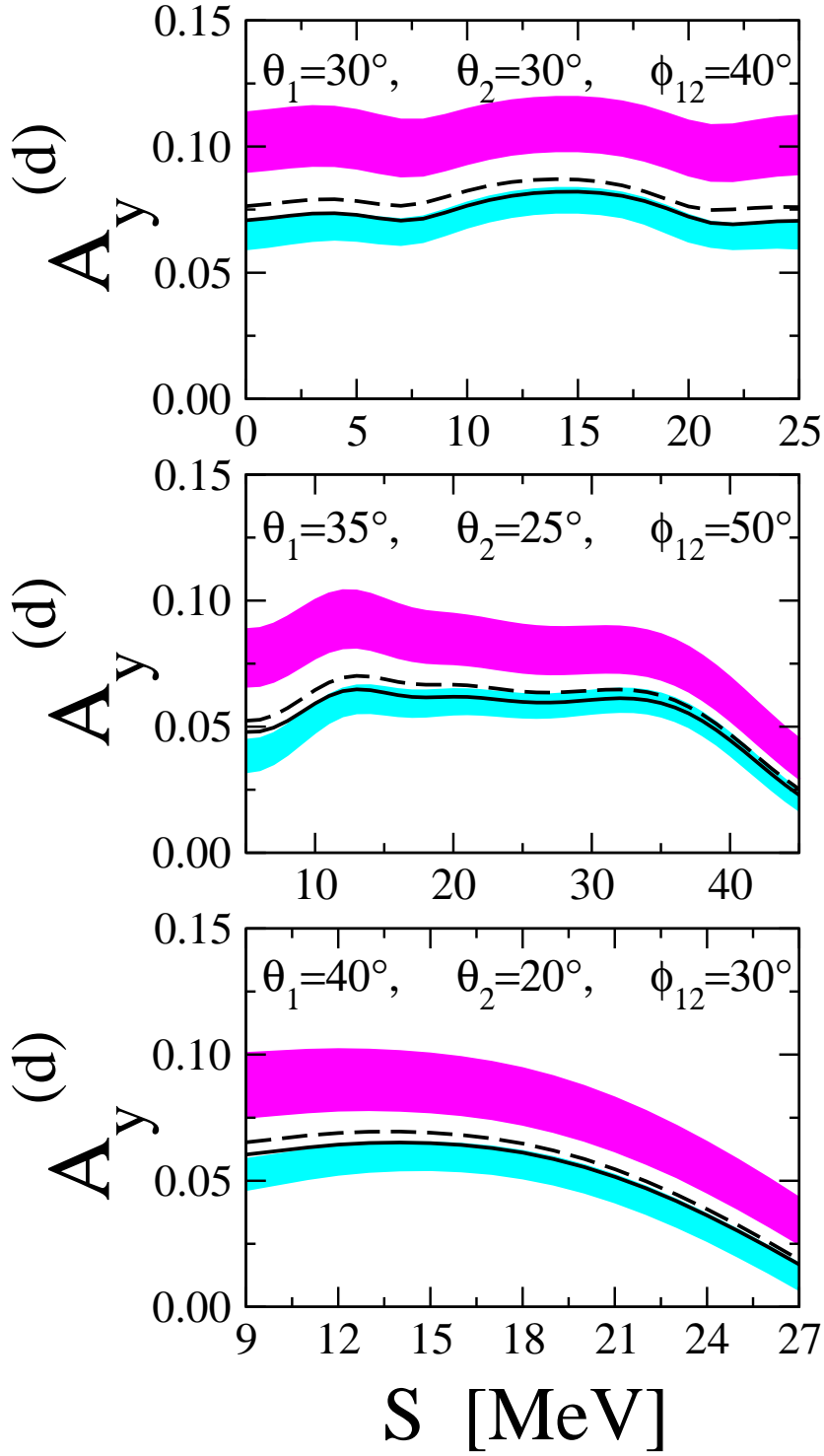


FIG. 19. Theoretical predictions for the deuteron vector analyzing power $A_y^{(d)}$ of the dN breakup at 130 MeV for selected configurations. For the description of bands and lines see caption of Fig. 18.

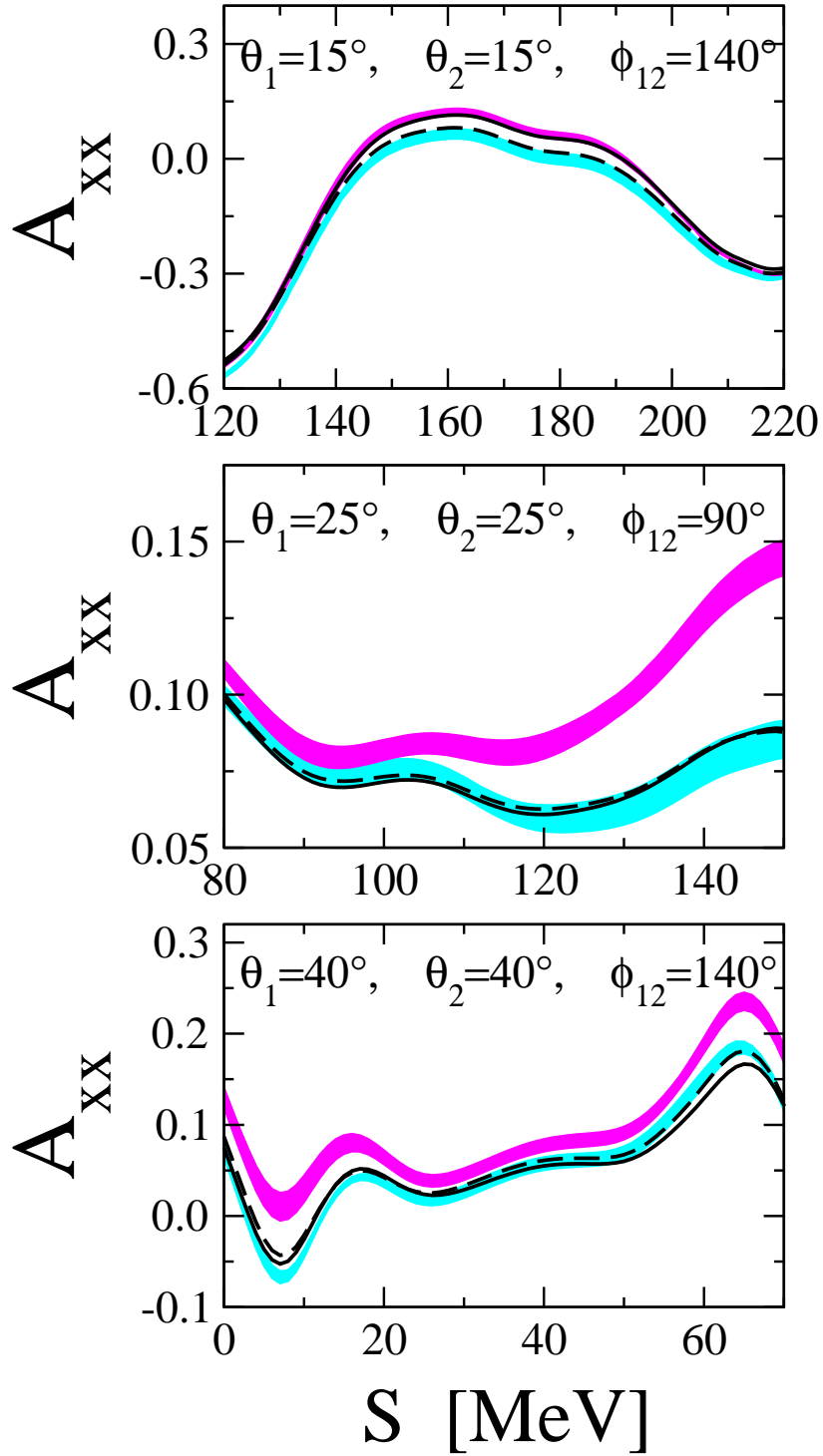


FIG. 20. Theoretical predictions for the tensor analyzing power A_{xx} of the dN breakup at 130 MeV for selected configurations. For the description of bands and lines see caption of Fig. 18.

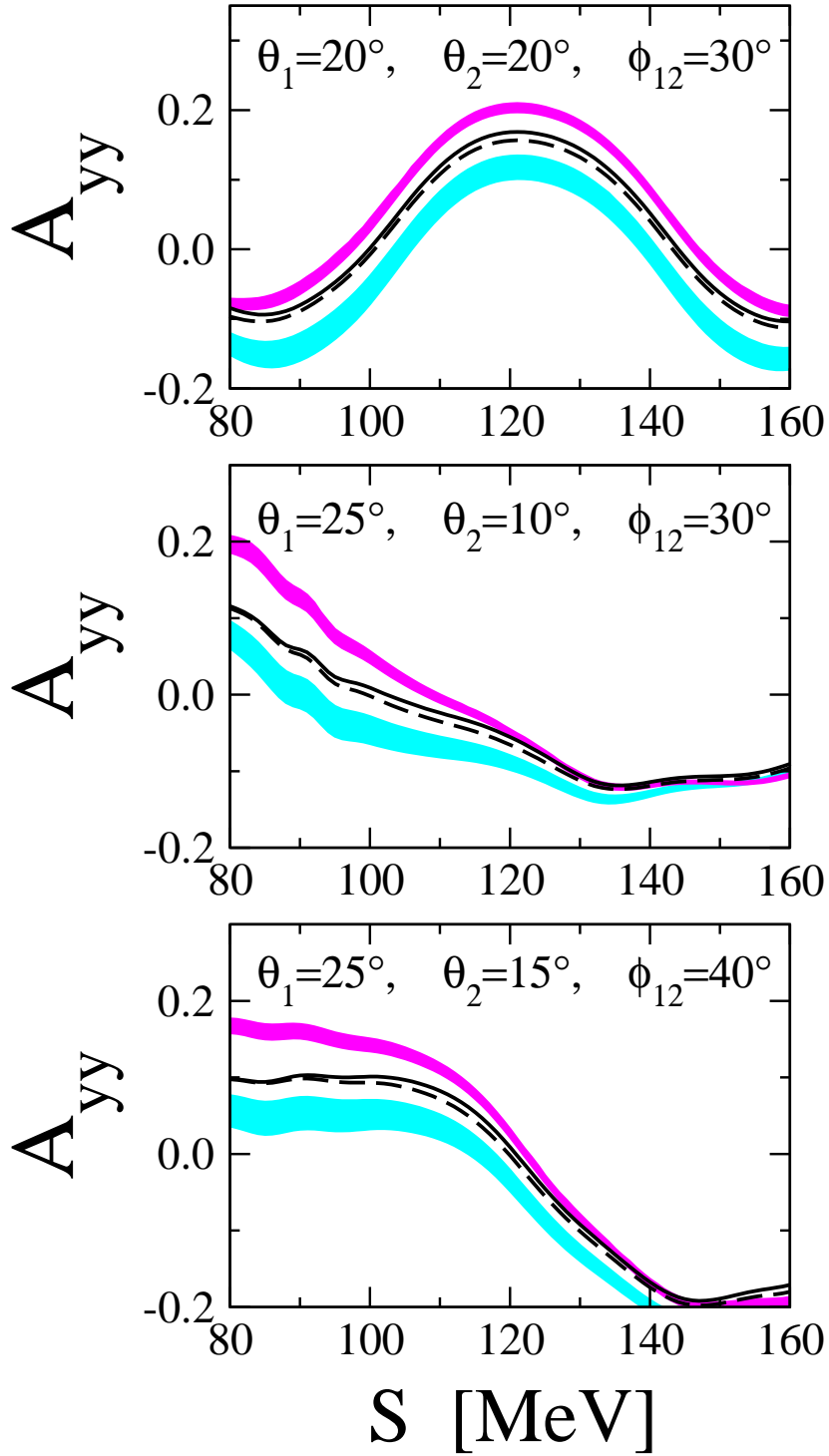


FIG. 21. Theoretical predictions for the tensor analyzing power A_{yy} of the dN breakup at 130 MeV for selected configurations. For the description of bands and lines see caption of Fig. 18.

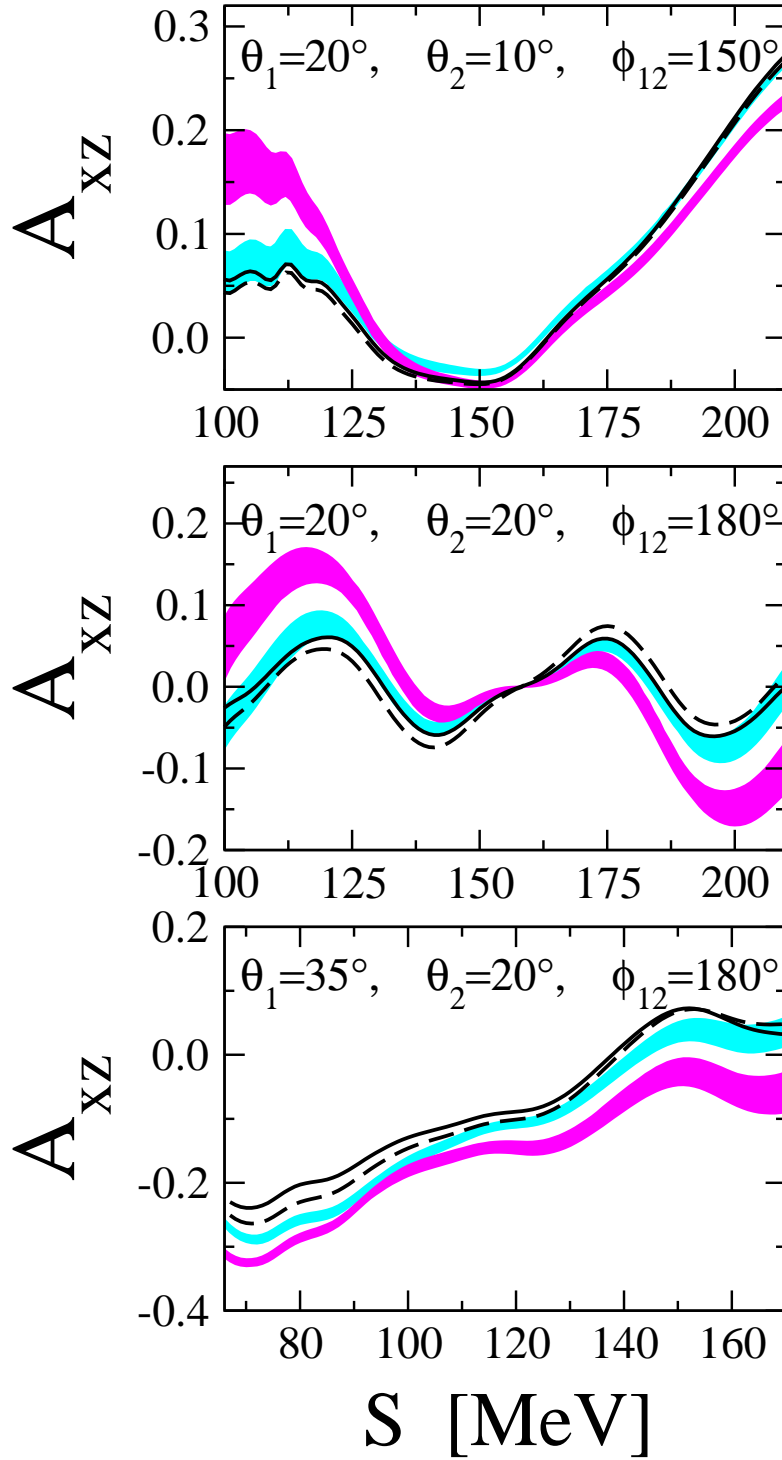


FIG. 22. Theoretical predictions for the tensor analyzing power A_{xz} of the dN breakup at 130 MeV for selected configurations. For the description of bands and lines see caption of Fig. 18.

This figure "break_partI_fig7.gif" is available in "gif" format from:

<http://arxiv.org/ps/nucl-th/0203017v1>

This figure "break_partI_fig8.gif" is available in "gif" format from:

<http://arxiv.org/ps/nucl-th/0203017v1>